nature chemistry

Article

https://doi.org/10.1038/s41557-023-01417-5

Structural characterization and reactivity of a room-temperature-stable, antiaromatic cyclopentadienyl cation salt

In the format provided by the authors and unedited

Table of Contents

I. Synthetic Details

Caution! Pentafluorophenyl copper and the complex of pentafluorophenylmagnesium bromide with diethyl ether have not, to the best of our knowledge, been reported to be explosive. However, a variation of the preparation described here, in which the complex of pentafluorophenylmagnesium bromide with diglyme was dried *in vacuo*, resulted in a vigorous decomposition under pressure build-up which destroyed the apparatus. This happened only once although the preparation was carried out several times. Caution should be exercised because the exact cause of the decomposition is unknown. The following procedure avoids isolation of this complex.

Bis(pentafluorophenyl)ethyne B: 400 mmol (9.72 g) of magnesium turnings were suspended in diethyl ether (133 mL). At 0 °C 400 mmol (43.59 g, 29.9 mL) bromoethane was slowly added to this suspension. The resulting mixture was warmed to room temperature and stirred overnight. The light gray solution was cooled to 0 °C and 400 mmol (98.78 g, 50.65 mL) of bromopentafluorobenzene, 500 mmol (67.1 g, 71.4 mL) of diglyme (diethylene glycol dimethyl ether), and 400 mmol (57 g) of CuBr were slowly added in sequence. The resulting white semi-solid mass was dried *in vacuo* for 1 h and then re-suspended in 400 mL diglyme. 100 mmol (9.76 mL, 26.47 g) of tribromoethylene was added slowly at 0 °C. The suspension slowly turned brown upon stirring at 120 °C for 24 h. It was then diluted on air with 500 mL ethyl acetate, 100 mL saturated $NH_4Cl_{(aq)}$ solution, 40 mL acetic acid, and 200 mL H_2O. The aqueous phase was discarded, and the organic phase was washed five times with H_2O. It was then dried with $MgSO_4$, concentrated on a rotary evaporator, and stripped of any remaining volatiles at 10^{-3} mbar. A by-product (probably decafluorobiphenyl) was removed by sublimation at 60 °C/10^{-3} mbar. The remaining crude product was crystallized from methanol at –30 °C.

Yield 14.4 g, 40.1 mmol, 40 %. **Mp** 123 °C. **^{19}F NMR** (376 MHz, C_6D_6): δ –135.61 to –135.75 (m, 4F, *ortho*), –150.34 (t, 2F, $^3J_{FF}$ = 22.0 Hz, *para*), –161.29 to –161.47 (m, 4F, *meta*). The melting point is consistent with the literature.[1]

Comments: The protocol was adapted from a literature procedure.[2] In contrast to Webb and Gilman, we found a higher reaction temperature and the use of diglyme instead of THF more convenient due to the shorter reaction time. The aqueous workup prevents the formation of finely divided Cu_2O, which is otherwise difficult to remove by filtration.

Tetrakis(pentafluorophenyl)cyclopentadienone C: 40.1 mmol (14.4 g) of bis(pentafluorophenyl)ethyne and 42.1 mmol (14.4 g) of $Co_2(CO)_8$ were suspended in decaline (100 mL) and stirred until gas evolution has stopped (4 h). The solution was then stirred at 190 °C for 24 h to form a metal mirror. The flask was cooled to room temperature, the solution was diluted with 100 mL of ethyl acetate and 86.3 mmol (21.9 g) of I_2 was added. The suspension was stirred until dissolution of the metal mirror and complete cessation of gas evolution (15 min). The solution was diluted with ethyl acetate (500 mL) and washed with aqueous $NaHSO_3$ solution (200 mL, 30 %). The aqueous phase was discarded. The organic phase was dried with $MgSO_4$ and filtered over about 50 mL of active Al_2O_3. All volatiles were removed first on a rotary evaporator and then by distillation at up to 160 °C/10^{-3} mbar. The product was then washed with 100 mL of *n*-hexane at –78 °C and recrystallized from $CHCl_3$ at –30 °C.

Yield 12.0 g, 16.1 mmol, 80 %. **Mp** 231 °C **^{19}F NMR** (376 MHz, C_6D_6): δ –137.57 to –137.82 (m, 8F, *ortho*), –145.76 (t, 2F, $^3J_{FF}$ = 21.6 Hz, *para*), –147.97 (t, 2F, $^3J_{FF}$ = 21.6 Hz, *para*), –157.96 to –158.17 (m, 4F, *meta*), –159.25 to –159.44 (m, 4F, *meta*). The melting point is consistent with the literature.[3]

Comments: Variations of this procedure omitting the oxidation step have been known for a long time,[4,5] but in our hands the main product of these reactions was a cobalt-containing complex of unknown structure. Oxidation of this complex with iodine yields the desired product.

Pentakis(pentafluorophenyl)cyclopentadienol D: 19.3 mmol (4.77 g, 2.41 mL) of bromopentafluorobenzene was slowly added at 0 °C to a solution of 19.3 mmol (6.44 mL) EtMgBr in diethyl ether (3 mol/L). All volatiles were removed under vacuum and the resulting colorless solid was redissolved in THF (10 mL). This solution was slowly added at –78 °C to a suspension of tetrakis(pentafluorophenyl)cyclopentadienone (16.1 mmol, 12.0 g) in THF (100 mL). The resulting mixture was gradually warmed to 25 °C within 4 h. Then 3 mL HCl_{aq} (37 %), 100 mL diethyl ether, and 100 mL of water were added. The aqueous phase was discarded and the organic phase was washed with 100 mL of water. The solution was dried with $MgSO_4$ and all volatiles were removed under reduced pressure using a rotary evaporator. The product was purified by column chromatography (*n*-hexane/diethyl ether 20:1; R_f = 0.30; colorless band with a blue fluorescence).

Yield 10.3 g, 11.3 mmol, 58 %. **Mp** 216 °C. **^{19}F NMR** (565 MHz, CD_2Cl_2): δ –134.96 (br s, 1F, $HOCC_6F_5$, *ortho*), –137.97 (br s, not integratable, $HOCCCC_6F_5$, *ortho*) –138.92 (m, 2F, $HOCCC_6F_5$, *ortho*), –139.53 (d, 2F, $^3J_{FF}$ = 21.7

Hz, $HOCCC_6F_5$, *ortho*), –144.02 (d, 2F, $^3J_{FF}$ = 21.3 Hz, $HOCC_6F_5$, *ortho*), –150.01(t, 2F, $^3J_{FF}$ = 20.8 Hz, $HOCCC_6F_5$ or $HOCCCC_6F_5$, *para*), –150.10 (t, 2F, $^3J_{FF}$ = 21.0 Hz, $HOCCC_6F_5$ or $HOCCCC_6F_5$, *para*), –152.60 (t, 1F, $^3J_{FF}$ = 21.2 Hz, $HOCC_6F_5$, *para*), –159.73 (td, 2F, $^3J_{FF}$ = 21.7 Hz, 7.7 Hz, $HOCCC_6F_5$, *meta*), –159.85 (td, 2F, $^3J_{FF}$ = 21.8 Hz, 7.7 Hz, $HOCCC_6F_5$, *meta*), –160.08 (td, 2F, $^3J_{FF}$ = 21.7 Hz, 7.7 Hz, $HOCCCC_6F_5$, *meta*), –160.45 (br t, 2F, $^3J_{FF}$ = 21.4 Hz, $HOCC_6F_5$, *meta*), –162.30 (br t, 2F, $^3J_{FF}$ = 20.9 Hz, $HOCC_6F_5$, *meta*). **^{1}H NMR** (400 MHz, C_6D_6): δ 3.40 (s, CpOH). **^{13}C{^{19}F} NMR** (151 MHz, CD_2Cl_2): δ 148.04 ($HOCC_6F_5$, *ortho*), 145.24 ($HOCCCC_6F_5$, *ortho*), 144.86 ($HOCC_6F_5$, *ortho*), 144.48 ($HOCCC_6F_5$, *ortho*), 144.35 ($HOCCC_6F_5$, *ortho*), 142.72 ($HOCCC_6F_5$ or $HOCCCC_6F_5$, *para*), 142.65 ($HOCCC_6F_5$ or $HOCCCC_6F_5$, *para*), 141.84, 141.83, 141.76 ($HOCC_6F_5$, *para*), 138.77 ($HOCC_6F_5$, *meta*), 138.26 ($HOCCCC_6F_5$, *meta*), 138.20 ($HOCCC_6F_5$, *meta*), 138.09 ($HOCC_6F_5$, *meta*), 137.86 ($HOCC_6F_5$, *meta*), 135.85 (HOCCC), 109.43 (HOCC), 106.76 ($HOCC_6F_5$ or $HOCCC_6F_5$, *ipso*), 106.36 ($HOCC_6F_5$ or $HOCCC_6F_5$, *ipso*), 90.36 (HOC). **ATR-IR**: ν = 3601, 1646, 1514, 1484, 1341, 1305, 1118, 1088, 982, 912, 803, 731 cm^{-1}.

Pentakis(pentafluorophenyl)cyclopentadienyl hexadecafluorotriantimonate $1^+[Sb_3F_{16}]^-$: Pentakis(pentafluorophenyl)cyclopentadienyl radical **2** (10 µmol, 8.6 mg) and $SbF_5{\cdot}SO_2$ (40 µmol, 11.2 mg) were suspended in 0.5 mL of hexafluorobenzene. 200 µmol (33.9 mg) of XeF_2 was added and the mixture was stirred for 30 min at 25 °C, resulting in the formation of a colorless gas, a deep blue solution, and a blue precipitate. The solution was decanted from the solid by using a glass syringe, sealed in a glass ampoule, and stored at 6 °C for three days.

The first run of this reaction gave the solvate $Cp(C_6F_5)_5Sb_3F_{16}{\cdot}2\ C_6F_5$ (**$1b^+[Sb_3F_{16}]^-{\cdot}1C_6F_5$**), all subsequent runs gave $Cp(C_6F_5)_5Sb_3F_{16}{\cdot}1.5\ C_6F_5$ (**$1a^+[Sb_3F_{16}]^-{\cdot}1.5C_6F_5$**). The yield varied from 8.6 mg to 15.1 mg (47-81 %) for **$1a^+[Sb_3F_{16}]^-{\cdot}1.5C_6F_5$** and was not determined for **$1b^+[Sb_3F_{16}]^-{\cdot}1C_6F_5$**.

Alternative preparation: 10 µmol (9.1 mg) pentakis(pentafluorophenyl)cyclopentadienol **D** and 40 µmol (11.2 mg) $SbF_5{\cdot}SO_2$ were suspended in 0.5 mL hexafluorobenzene and stirred for 30 min at 25 °C, resulting in the formation of a deep blue solution and a blue precipitate. The solution was decanted from the solid using a glass syringe, and further treated as above, yielding crystals with identical cell parameters and color.

In situ NMR spectroscopy: Pentakis(pentafluorophenyl)cyclopentadienol **D** (10 µmol, 9.1 mg) was dissolved in 0.5 mL of SO_2 at –78 °C in a Teflon-capped NMR tube, which also contained a capillary with acetone-d_6 and the first NMR spectrum was measured at –30 °C. The solution was again cooled to –78 °C, 50 µmol (14.0 mg) $SbF_5{\cdot}SO_2$ were sublimed into the NMR tube, and the second NMR spectrum was measured at –30 °C.

Comments: The use of a glass syringe is necessary, because $\mathbf{1}^+$ reacts immediately with polypropylene syringes to form **2** and unidentified other products. An excess of XeF_2 is also necessary because $SbF_5{\cdot}SO_2$ catalyzes the reaction of XeF_2 with hexafluorobenzene. For the second preparation, starting from **D**, the formation of hydroxide-containing counteranions $Sb_3(OH)_nF_{(16-n)}$ cannot be completely excluded. Crystals for sc-XRD were therefore obtained from the first reaction (oxidation of **2**).

UV-Vis (hexafluorobenzene): λ_{max} (log ε) = 678 nm (4.68).

Caution! When XeF_2 and $SbF_5{\cdot}SO_2$ are premixed and the solvent is added subsequently, a vigorous reaction with flame formation may occur even in the absence of air.

Pentakis(pentafluorophenyl)cyclopentadienyl radical 2: 1 mmol (912 mg) pentakis(pentafluorophenyl)cyclopentadienol and 20 mmol (5.33 g) $AlBr_3$ were suspended in 3 mL of benzene and 10 mmol (1.09 g, 746 µL) of bromoethane was slowly added at 0 °C. The red suspension was warmed to 25 °C, stirred for 30 min, and subsequently cooled to 0 °C. The suspension was filtered, and the filtrate was discarded. The solid was quenched with 200 mmol (3.6 g) ice and the mixture was kept at 25 °C until completely thawed. The solution was then removed by filtration and the solid was washed rapidly three times with 10 mL of water at 0 °C. All volatiles were removed under reduced pressure and the solid was sublimed at 150 °C/10^{-3} mbar over 2 days. The sublimate was crystallized three times from 1 mL of toluene and again all volatiles were removed under vacuum.

Yield 484 mg, 541 µmol, 54 %. **Mp** 236 °C, evaporates undecomposed at approx. 300 °C. **ATR-IR**: ν = 1647, 1517, 1487, 1383, 1344, 1312, 1138, 1104, 1079, 983, 919, 911, 836, 730, 654, 542 cm^{-1}. **UV-Vis** (hexafluorobenzene): λ_{max} (log ε) = 546 nm (3.41).

Comments: The washing steps can be performed in a Büchner funnel without the need for an inert gas atmosphere, since crystalline **2** is stable under these conditions. The mother liquors and the liquid portion of the reaction mixture contain mainly pentakis(pentafluorophenyl)cyclopentadiene and can be used for the preparation of pyridinium pentakis(pentafluorophenyl)cyclopentadienide.

Ferrocenium pentakis(pentafluorophenyl)cyclopentadienide 3a: 5 µmol (4.5 mg) pentakis(pentafluorophenyl)cyclopentadienyl radical and 6 µmol (1.1 mg) ferrocene were dissolved in 0.3 mL 1,2-difluorobenzene. The product was crystallized by vapor phase diffusion with 3 mL of *n*-hexane.

Yield 3.5 mg, 3.2 µmol, 65 %. **Mp** 232 °C. **^{19}F NMR** (565 MHz, thf-d_8): δ –142.96 (dd, 10F, $^3J_{FF}$ = 25.2 Hz, $^4J_{FF}$ = 8.3 Hz, *ortho*), –163.13 (t, 5F, $^3J_{FF}$ = 21.5 Hz, *para*), –166.38 to –166.51 (m, 10F, *meta*). **^{13}C NMR** (151 MHz, CD_2Cl_2): δ 145.1 (d, $^1J_{FC}$ = 243 Hz, *meta*), 139.2 (d, $^1J_{FC}$ = 243 Hz, *para*), 138.3zz (dt, $^1J_{FC}$ = 246 Hz, *ortho*, $^2J_{FC}$ = 14.5 Hz), 116.7 (t, $^2J_{FC}$ = 19.3 Hz, *ipso*), 108.5 ($C_5(C_6F_5)_5$). **ATR-IR**: ν = 3111, 3075, 1514, 1471, 1418, 1282, 1267, 1098, 976, 915, 849, 759, 540 cm^{-1}.

Tritylium pentakis(pentafluorophenyl)cyclopentadienide 3b: 5 µmol (4.5 mg) of pentakis(pentafluorophenyl)cyclopentadienyl radical and 3 µmol (1.7 mg) of trityl$_2$·toluene were heated to 110 °C in 0.5 mL of toluene until all solids were dissolved (about 10 min). The solution was then slowly cooled to 25 °C and left undisturbed for 24 h, resulting in the formation of large yellow-green needles.

Yield 4.9 mg, 4.4 µmol, 87 %. **Mp** 227 °C. **^{19}F NMR** (565 MHz, CD_2Cl_2): δ –142.71 (dd, 10F, $^3J_{FF}$ = 25.6 Hz, $^4J_{FF}$ = 7.4 Hz, *ortho*), –161.53 (t, 5F, $^3J_{FF}$ = 21.5 Hz, *para*), –164.97 to –165.16 (m, 10F, *meta*). **^{1}H NMR** (400 MHz, CD_2Cl_2): δ 7.91 (br s). The signals in the ^{13}C NMR spectrum were too broad to be well resolved. **ATR-IR**: ν = 2945, 1574, 1516, 1479, 1350, 1290, 1181, 1099, 982, 916, 839, 764, 701, cm^{-1}.

Decamethylaluminocenium pentakis(pentafluorophenyl)cyclopentadienide 3c: 5 µmol (4.5 mg) of pentakis(pentafluorophenyl)cyclopentadienyl radical and 10 µmol (1.6 mg) of Cp*Al were heated to 110 °C in 0.5 mL of toluene until all reagents dissolved (about 10 min). This process was accompanied by the formation of a gray, finely dispersed solid (probably aluminum metal). The solution was then cooled to 25 °C. The grayish solid formed was isolated by centrifugation and extracted with 0.5 mL CH_2Cl_2. The extract was evaporated to dryness at 25 °C/10^{-3} mbar.

The formation of single crystals was achieved by immersing the product in a small glass tube (5 mm diameter) containing 1 mL of benzene and heating the lower end of the solution to 80 °C, while keeping the upper end at 25 °C.

Yield 5.3 mg, 4.9 µmol, 89 % (before crystallization). **Mp** 230 °C. **^{19}F NMR** (565 MHz, CD_2Cl_2): δ –142.74 (dd, 10F, $^3J_{FF}$ = 25.5 Hz, $^4J_{FF}$ = 7.0 Hz, *ortho*), –161.57 (t, 5F, $^3J_{FF}$ = 21.0 Hz, *para*), –165.04 to –165.17 (m, 10F, *meta*). **^{1}H NMR** (600 MHz, CD_2Cl_2): δ 2.16. **^{13}C NMR** (151 MHz, CD_2Cl_2): δ 144.4 (d, $^1J_{FC}$ = 241 Hz, *meta*), 138.9 (d, $^1J_{FC}$ = 248 Hz, *para*), 137.8 (dt, $^1J_{FC}$ = 248 Hz, *ortho*, $^2J_{FC}$ = 14.0f Hz), 119.3 (C_5Me_5), 115.5 (t, $^2J_{FC}$ = 19.3 Hz, *ipso*), 107.9 ($C_5(C_6F_5)_5$) 10.4 (C_5Me_5). **^{27}Al NMR** (156 MHz, CD_2Cl_2): δ 114.4. **ATR-IR**: ν = 2952, 2914, 2867, 1514, 1481, 1098, 982, 916, 653, 623, 574, 538 cm^{-1}.

Comments: The unusual shape of the ^{1}H NMR signal has been reported previously.[5]

Pyridinium pentakis(pentafluorophenyl)cyclopentadienide 3d: The combined mother liquors of **2**, including the soluble fraction of the reaction mixture, were washed with dilute hydrochloric acid (1 mol/L), dried with $MgSO_4$, and degassed by three freeze-thaw-pump cycles. 1 mmol (79.1 mg; 80.7 µL) of pyridine was added, initiating the formation of a colorless precipitate, which was removed by filtration, washed three times with 3 mL of benzene, and dried under reduced pressure.

Yield 302 mg, 314 µmol, 31 % (with respect to reagent **D**). **Mp** 218 °C. **^{19}F NMR** (565 MHz, thf-d_8): δ –143.02 (dd, 10F, $^3J_{FF}$ = 24.6 Hz, $^4J_{FF}$ = 7.7 Hz, *ortho*), –162.62 (t, 5F, $^3J_{FF}$ = 21.3 Hz, *para*), –166.03 to –166.22 (m, 10F, *meta*). **^{1}H NMR** (400 MHz, thf-d_8): δ 8.56 to 8.53 (m, 2H, *ortho*), 7.56 (tt, 1H, $^3J_{HH}$ = 7.6 Hz, $^4J_{HH}$ = 1.l9 Hz, *para*) 7.27 to 7.23 (m, 2H, *meta*). The signals in the ^{13}C NMR spectrum were too broad to be well resolved. **ATR-IR**: ν = 1516, 1474, 1099, 978, 915, 750, 691, 620, 538 cm^{-1}.

Pentakis(pentafluorophenyl)cyclopentadienylcarboxylic acid 5: 10 µmol (15.6 mg) of **1** was suspended in 0.5 mL of C_6F_6. The solution was degassed and 89 µmol (2 mL; 1.1 bar; 25 °C) of CO was added. The solution was stirred for 24 h, resulting in a color change from deep blue to pale yellow and the formation of brown solids. All volatiles were removed under vacuum. 1 mL of water and 1 mL of benzene were added to the solid residue. The phases were separated, the aqueous phase was discarded, and the organic phase was dried with $MgSO_4$. All volatiles were removed again under vacuum.

The product is a mixture of **5** and **6**, since **5** decomposes slowly to **6** under the conditions of the work-up and NMR measurement. Single crystals of **5** were obtained by vapor phase diffusion of *n*-hexane into a concentrated solution of **5** in hexafluorobenzene at 6 °C.

Yield 7 mg. **^{19}F NMR** (565 MHz, C_6D_6): δ –132.34 (br s, 1F, *ortho*), –135.05 (br s, 1F, *ortho*), –138.42 (d, 2F, $^3J_{FF}$ = 21.6 Hz, *ortho*), –139.28 to –139.48 (m, not integratable due to overlap and uneven baseline, *ortho*), –145.35 (t,

2F, $^3J_{FF}$ = 21.7 Hz, *para*), –146.33 (d, 2F, $^3J_{FF}$ = 21.7 Hz, *para*), –148.23 (d, 2F, $^3J_{FF}$ = 21.7 Hz, *para*), –158.0 to –158.41 (m, 9F, *meta*) –160.05 (td, 1H, $^3J_{FF}$ = 21.7 Hz, $^4J_{FF}$ = 6.1 Hz, *meta*).

Comment: Because **5** decomposes during column chromatography and on prolonged standing, only the ^{19}F NMR spectrum and sc-XRD data are reported.

Pentakis(pentafluorophenyl)cyclopentadiene 6: 5 µmol of **3a**, **3b**, or **3c** are suspended in 1 mL of hydrochloric acid (1 mol/L). The suspension is extracted three times with 1 mL of dichloromethane (DCM). The combined extracts are dried with $MgSO_4$ and all volatiles are removed under reduced pressure (3 h to ensure the removal of ferrocene, Cp*H, and pyridine). The yield is almost quantitative.

If larger amounts of **6** are desired, the following procedure is advantageous: 0.5 mmol (456 mg) pentakis(pentafluorophenyl)cyclopentadienol and 10 mmol (2.67 g) $AlBr_3$ were suspended in 1.5 mL benzene and 5 mmol (0.55 g, 373 µL) bromoethane was slowly added at 0 °C. The red suspension was warmed to 25 °C and stirred for 30 min. The suspension was quenched with 100 mmol (1.8 g) ice and the mixture was kept at 25 °C until completely thawed. 0.5 mmol (93 mg) ferrocene and 1.5 mL hydrochloric acid (1 mol/L) were added and the suspension was stirred for 30 min. It was then diluted with 10 mL DCM and the phases were separated. The aqueous phase was discarded and the organic phase was dried with $MgSO_4$. All volatiles were removed under vacuum. The crude product was dissolved in 5 mL hot toluene and hot filtered. 0.5 mmol (39.6 mg; 40.6 µL) pyridine was added to the filtrate and the solution was stored at 25 °C for 24 h. The separated solids were isolated by filtration and dissolved in a mixture of 1.5 mL hydrochloric acid (1 mol /L) and 10 mL DCM. The aqueous phase was discarded and the organic phase was dried with $MgSO_4$. All volatiles were removed under vacuum.

Yield 309 mg, 345 mmol, 69 %. **Mp** 188 °C (dec.). **^{19}F NMR** (565 MHz, C_6D_6): δ –139.13 (d, 2F, $^3J_{FF}$ = 21.0 Hz, $HCCC_6F_5$, *ortho*), –140.00 (d, 4F, $^3J_{FF}$ = 21.2 Hz, $HCCCC_6F_5$, *ortho*), –140.62 (d, 2F, $^3J_{FF}$ = 23.0 Hz, $HCCC_6F_5$, *ortho*), –141.18 (d, 1F, $^3J_{FF}$ = 18.2 Hz, HCC_6F_5, *ortho*), –143.18 (d, 2F, $^3J_{FF}$ = 21.6 Hz, HCC_6F_5, *ortho*), –147.69 (t, 2F, $^3J_{FF}$ = 21.7 Hz, $HCCC_6F_5$ or $HCCCC_6F_5$, *para*), –148.14 (t, 2F, $^3J_{FF}$ = 21.3 Hz, $HCCC_6F_5$ or $HCCCC_6F_5$, *para*), –149.62 (t, 1F, $^3J_{FF}$ = 21.5 Hz, HCC_6F_5, *para*), –158.72 to –158.93 (m, 6F, *meta*), –159.18 to –159.42 (m, 3F, *meta*), –159.67 (td, 1F, $^3J_{FF}$ = 21.6 Hz, $^4J_{FF}$ = 8 Hz, HCC_6F_5, *meta*). **^{1}H NMR** (400 MHz, C_6D_6): δ 5.91 (s, CpH). **^{13}C{^{19}F} DEPT-135 NMR** (151 MHz, C_6D_6): δ 146.41 (d, $^3J_{HC}$ = 7.1 Hz HCC_6F_5, *ortho*), 145.94 (d, $^3J_{HC}$ = 5.7 Hz HCC_6F_5, *ortho*), 144.86 (s, $HCCC_6F_5$, *ortho*), 144.67 (s, $HCCCC_6F_5$, *ortho*), 144.31 (s, $HCCC_6F_5$, *ortho*), 142.47 (s, $HCCC_6F_5$ or $HCCCC_6F_5$, *para*), 142.31 (s, $HCCCC_6F_5$ or $HCCC_6F_5$, *para*), 142.08 (s, HCC_6F_5, *para*), 138.24 (s, $HCCC_6F_5$, *meta*), 138.21 (s, HCC_6F_5, *meta*), 138.18 (s, $HCCCC_6F_5$, *meta*), 138.17 (s, $HCCC_6F_5$, *meta*), 138.04 (s, $HCCCC_6F_5$, *meta*), 137.06 (s, HCC_6F_5, *meta*). **^{13}C{^{1}H} NMR** (151 MHz, C_6D_6): δ 146 to 136 (several multiplets) 107.84 - 106.83 (m, *ipso*), 53.56 (s, H*C*). **ATR-IR**: ν = 1656, 1522, 1491, 1445, 1315, 1105, 1080, 982, 935, 916, 841, 735, 652, cm^{-1}.

II. Spectroscopic Characterization

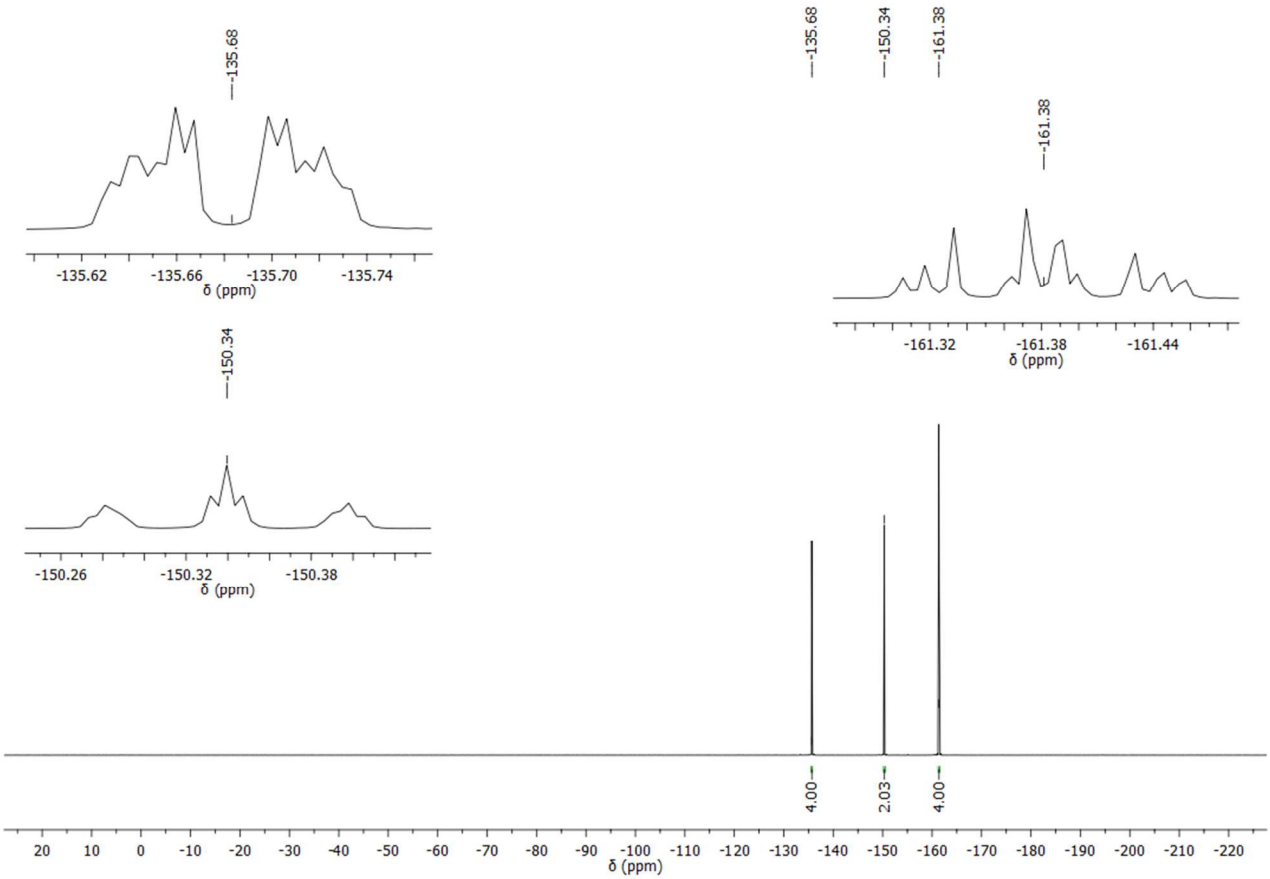

Figure S1. ^{19}F NMR spectrum of bis(pentafluorophenyl)ethyne **B** in C_6D_6 at 25 °C.

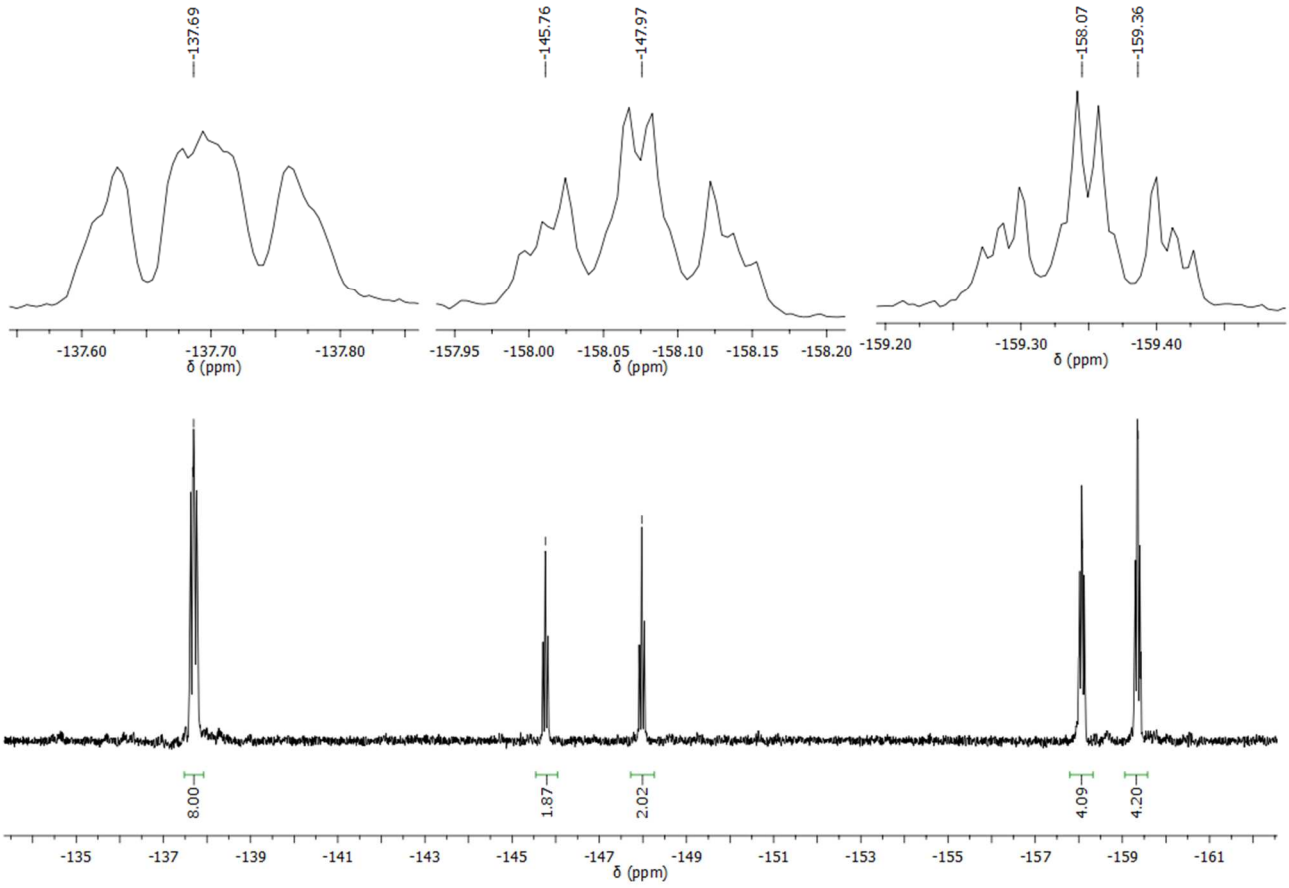

Figure S2. ^{19}F NMR spectrum of tetrakis(pentafluorophenyl)cyclopentadienone **C** in C_6D_6 at 25 °C.

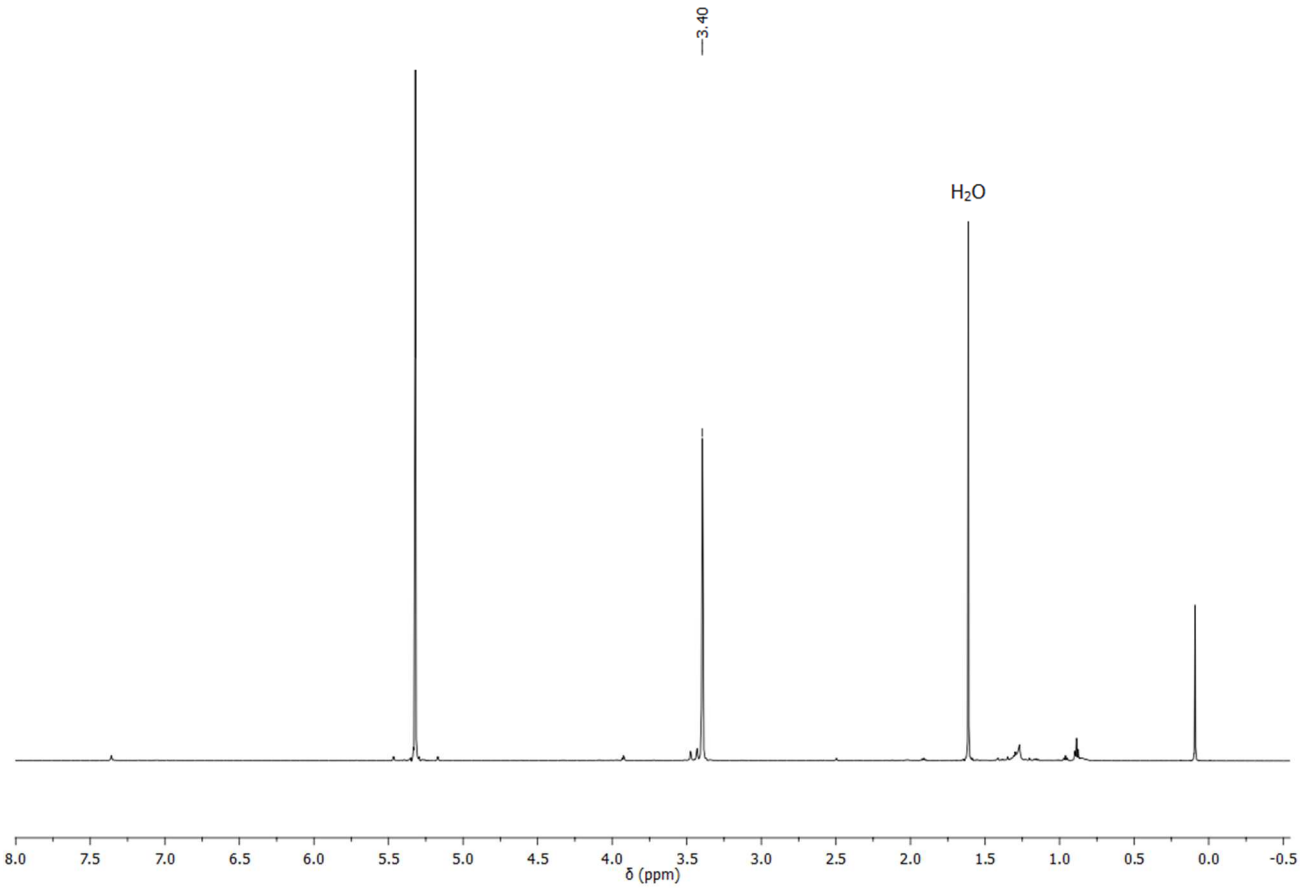

Figure S3. ^{1}H NMR spectrum of pentakis(pentafluorophenyl)cyclopentadienol **D** in CD_2Cl_2 at 25 °C.

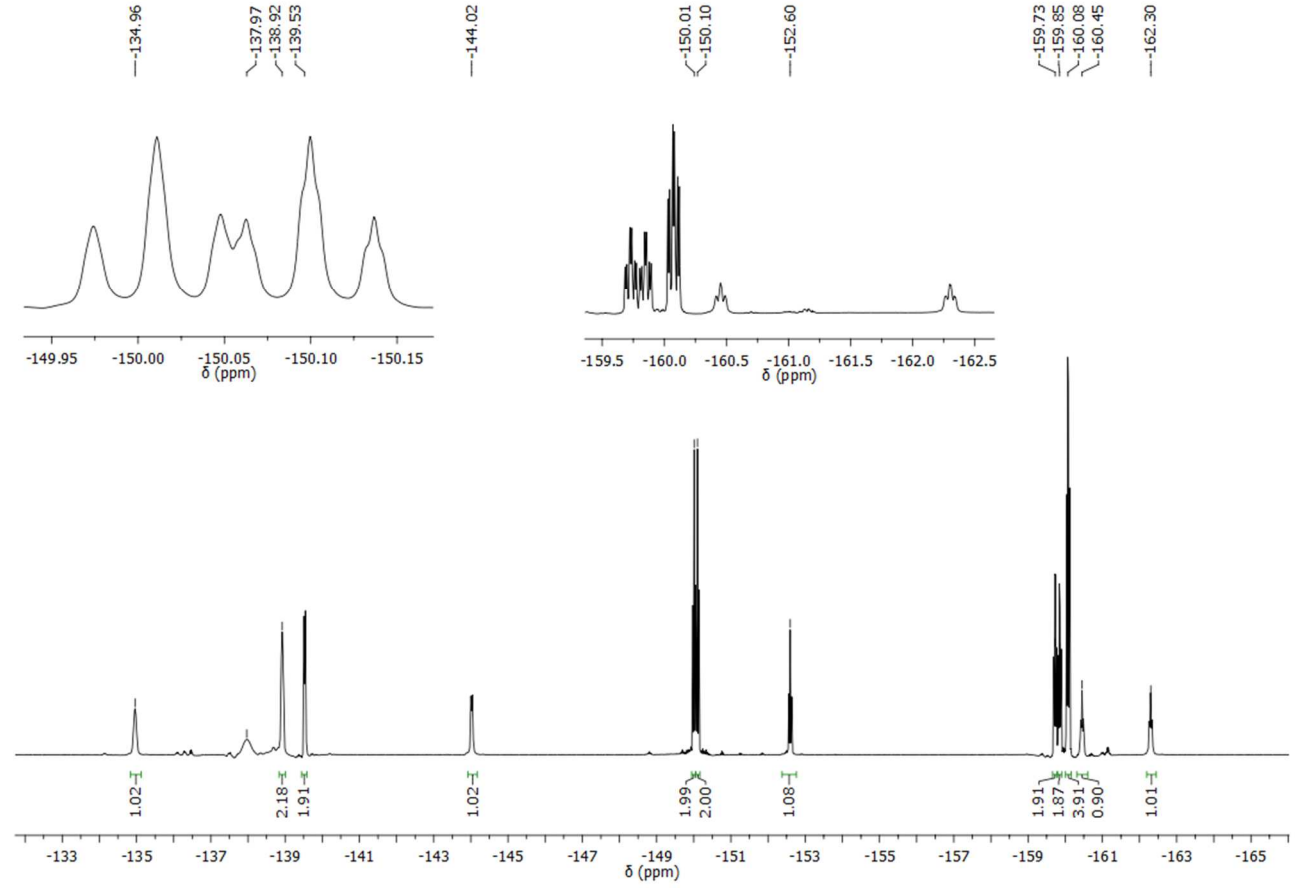

Figure S4. ^{19}F NMR spectrum of pentakis(pentafluorophenyl)cyclopentadienol **D** in CD_2Cl_2 at 25 °C.

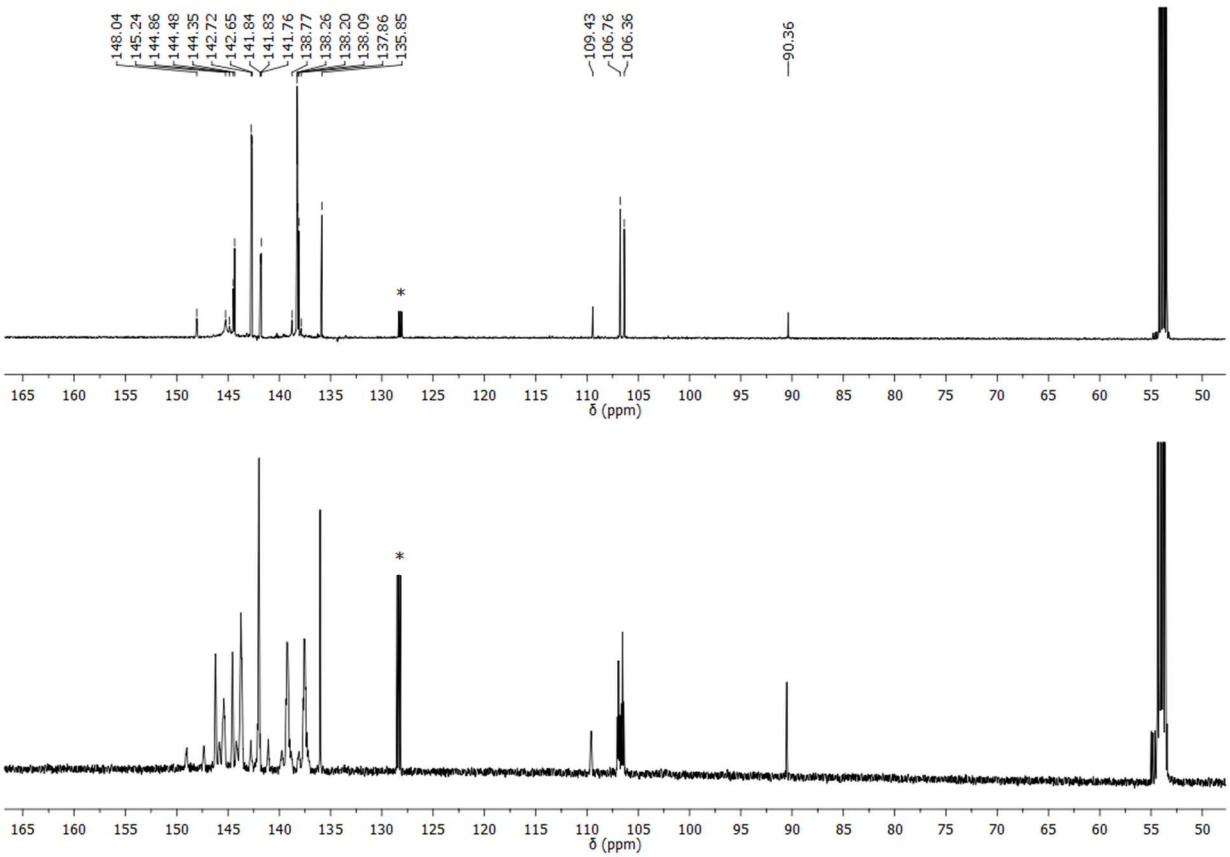

Figure S5. $^{13}C\{^{19}F\}$ NMR and $^{13}C\{^{1}H\}$ NMR spectrum of pentakis(pentafluorophenyl)cyclopentadienol **D** in CD_2Cl_2 at 25 °C (containing traces of C_6D_6 (*) from a previous measurement which was hindered by the low solubility in this solvent).

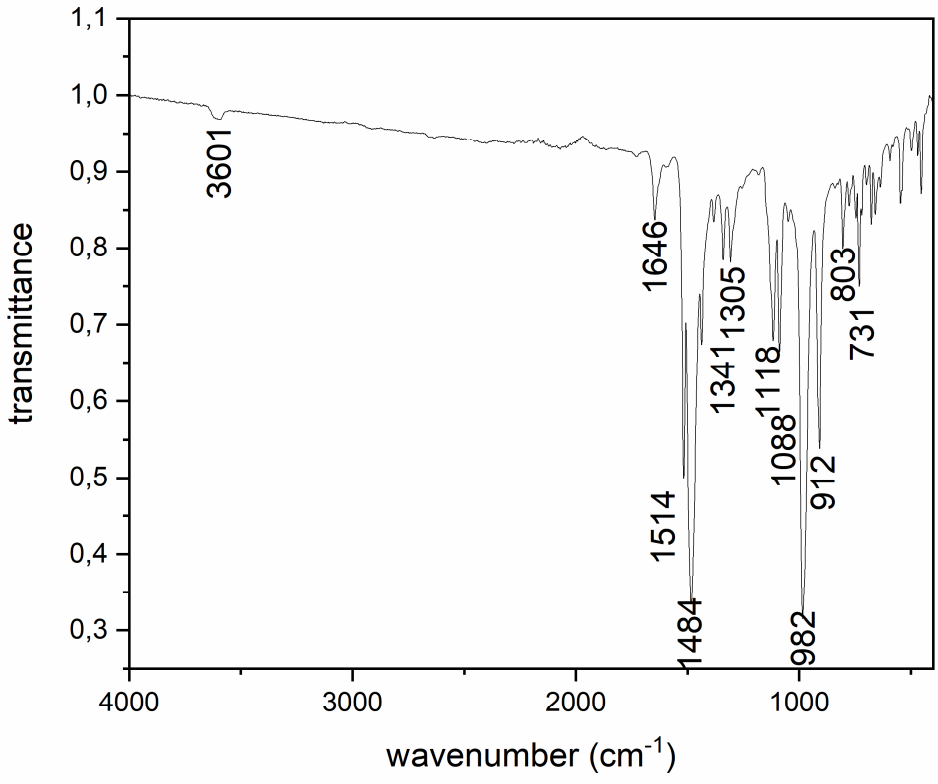

Figure S6. ATR-IR spectrum of pentakis(pentafluorophenyl)cyclopentadienol **D**.

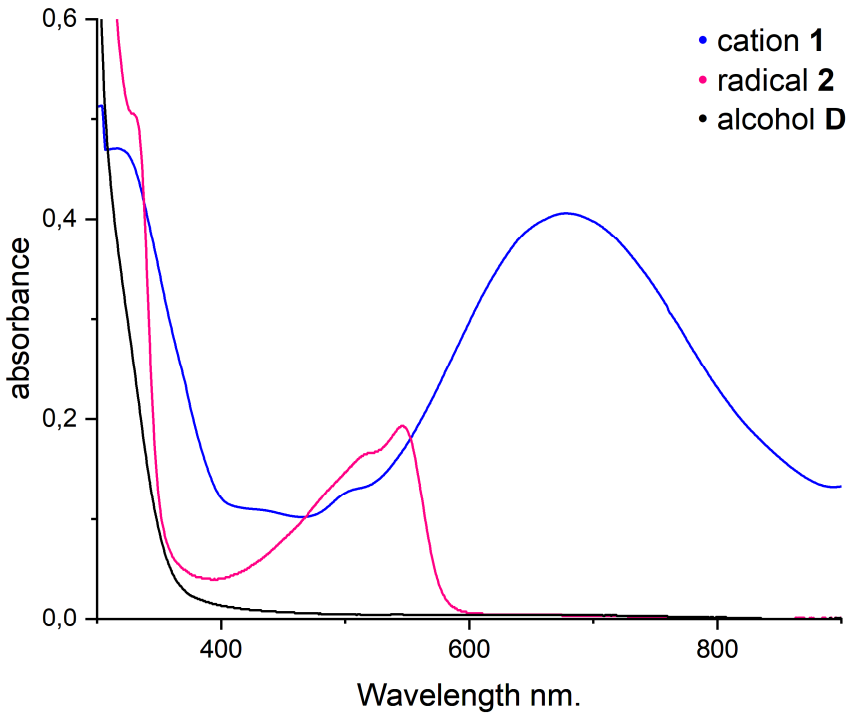

Figure S7. UV-vis spectra of cation $\mathbf{1}^+$, radical **2**, and alcohol **D** (50 µmol/L in hexafluorobenzene). The solution of **1** contained an excess (250 µmol/L) of $SbF_5 \cdot SO_2$ to scavange traces of reducing agents or nucleophiles. Quantitative results for **1** may be imprecise because the concentration of $\mathbf{1}^+$ was not accurately known due to difficulties in the handling of its solution.

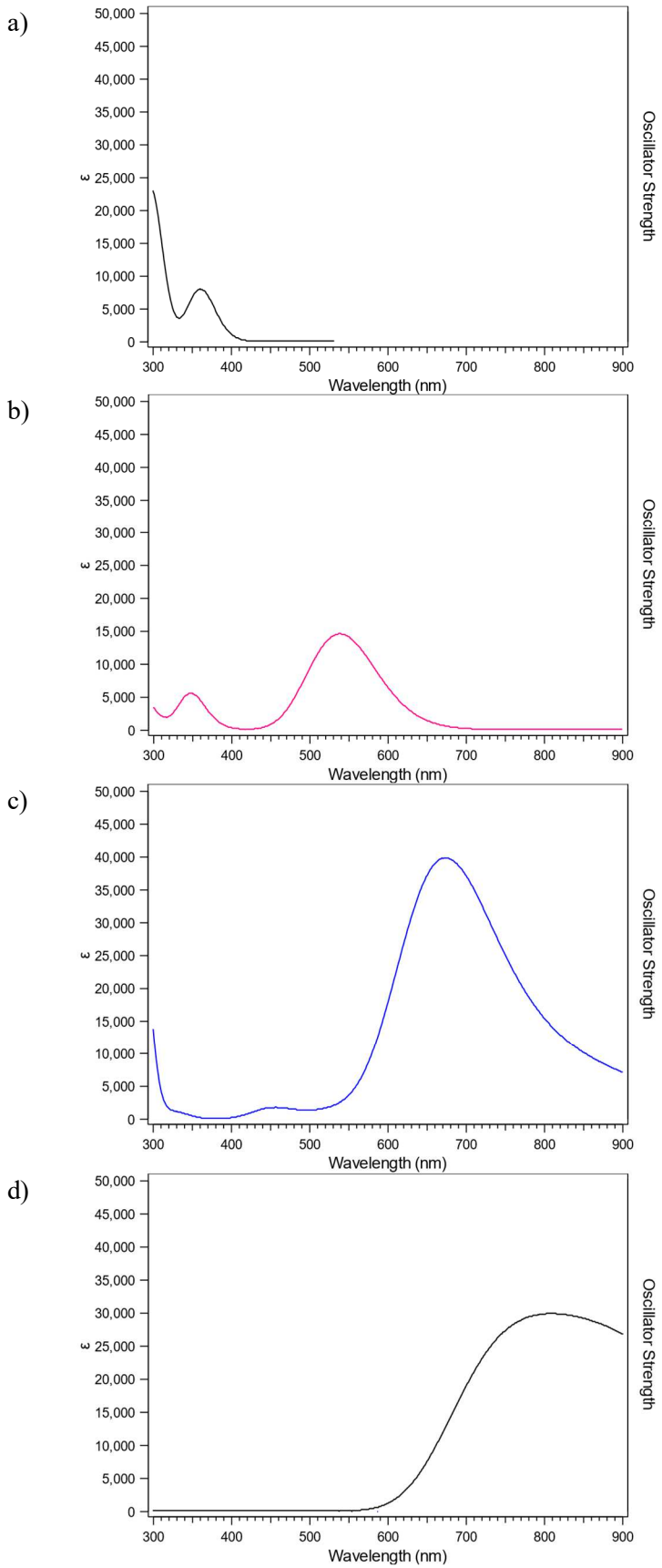

Figure S8. UV-visible spectra of cyclopentadiene **E** (a), radical **2** (b) as well as of the singlet (c) and triplet (d) state of $\mathbf{1}^{+}$ calculated at TD-PBE0(SMD,hexafluorobenzene)/def2-TZVP//B3LYP-D3BJ/TZP level of theory.

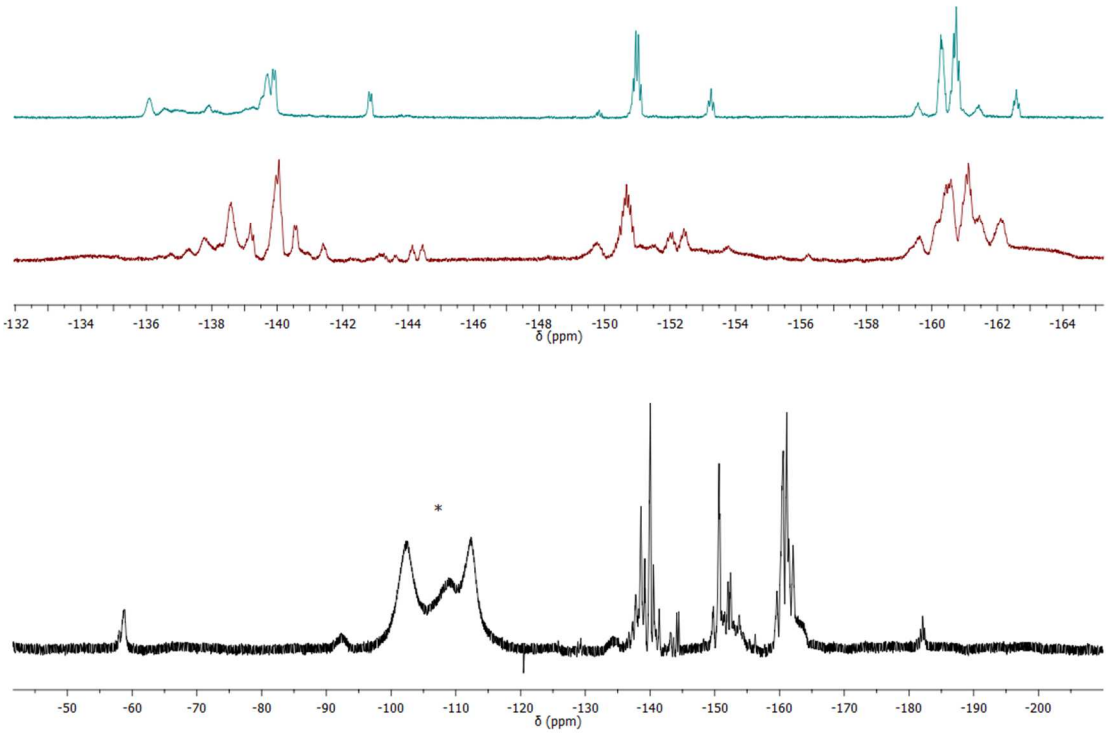

Figure S9. ^{19}F NMR spectra in liquid SO_2 at –30 °C of pentakis(pentafluorophenyl)cyclopentadienol **D** before (top, cyan) and after (middle, red and bottom, black) the addition of 5 equivalents of $SbF_5 \cdot SO_2$ using a glass capillary with acetone-d_6 as reference. The multiplet marked with an asterisk arises from $Sb_nF_mOH_o$ species.

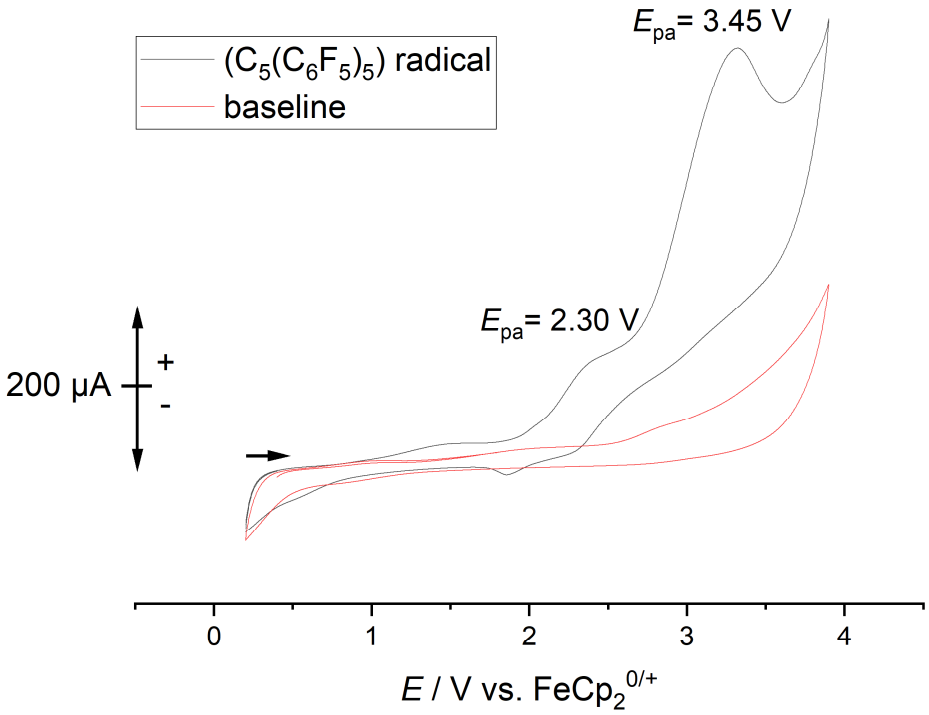

Figure S10. Cyclic voltammogram of the pentakis(pentafluorophenyl)cyclopentadienyl radical **2** at –20 °C in SO_2 with NBu_4SbF_6. We assign the first redox event at E_{pa} = 2.30 V to the oxidation of radical **2** to cation $\mathbf{1}^+$**.** The cause of the second redox event at E_{pa} = 3.45 V is unclear, but it is only observable in the presence of the sample and is possibly attributable to the subsequent oxidation of the aryl groups.

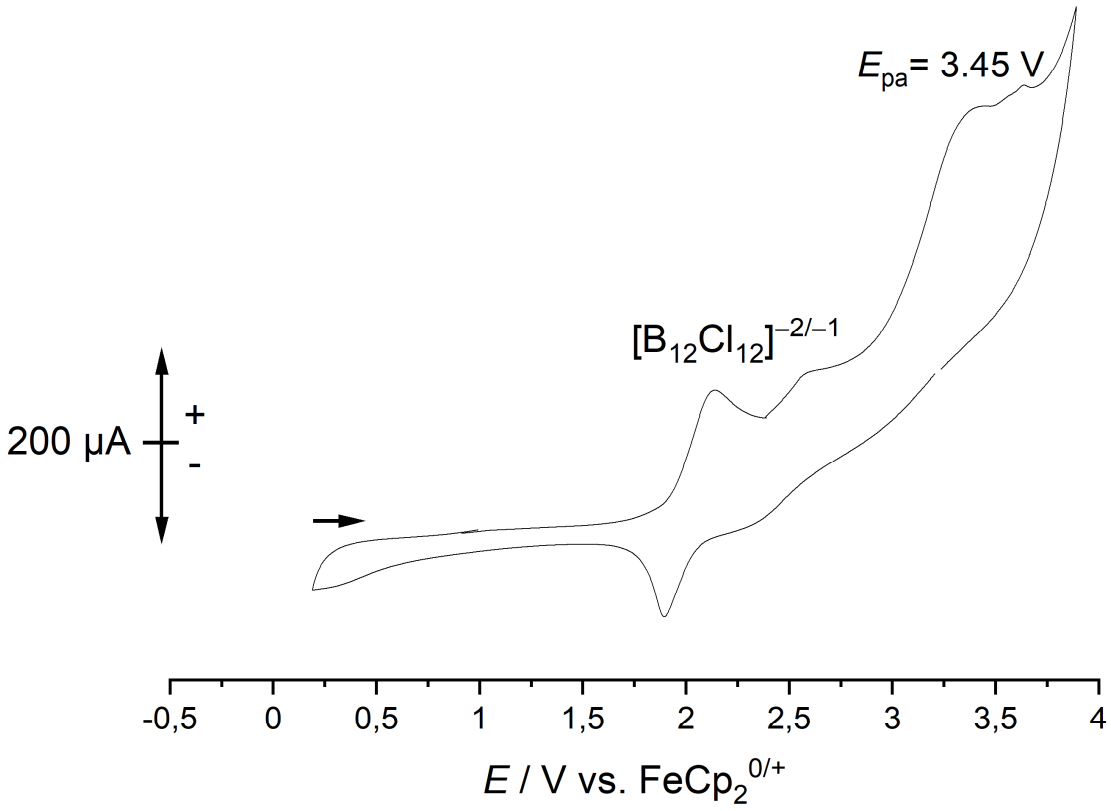

Figure S11. Cyclic voltammogram of the pentakis(pentafluorophenyl)cyclopentadienyl radical **2** with $Li_2B_{12}Cl_{12}$ as reference at –20 °C in SO_2 with NBu_4SbF_6.

Comments: The CV experiments in liquid SO_2 were performed starting with the Cp radical **2** from 0 V and going to the oxidation site. Two oxidation processes were observed above 2 V which were referenced with $Li_2B_{12}Cl_{12}$ against ferrocene. The boron cluster itself can be oxidized twice from the dianion to a monoanion at 2.11 V and from the monoanion to a neutral species at 2.67 V.[6] We assume that the first oxidation of the Cp radical takes places between the cluster oxidation processes. Due to the increased electric current of the second oxidation process (Fig. middle) in comparison to the cyclic voltammogram without the reference, we conclude that the Cp's potential is similar to the second oxidation of the cluster. A more accurate determination was attempted by referring the peak potential at E_{pa} = 3.45 V vs. ferrocene, which was repetitively observed in the experiments and is further on not interfering with the cluster processes, in the cyclic voltammograms without an internal reference yielding a peak potential of E_{pa} = 2.30 V vs. ferrocene of the Cp oxidation. However, it should be noted that due to the high reactivity of the generated species an unspecified decomposition of the mixture was observed during the second oxidation and reduction cycle in the referencing experiment. A possible oxidation of the conducting salt was ruled out by measuring the conducting salt alone (see baseline).

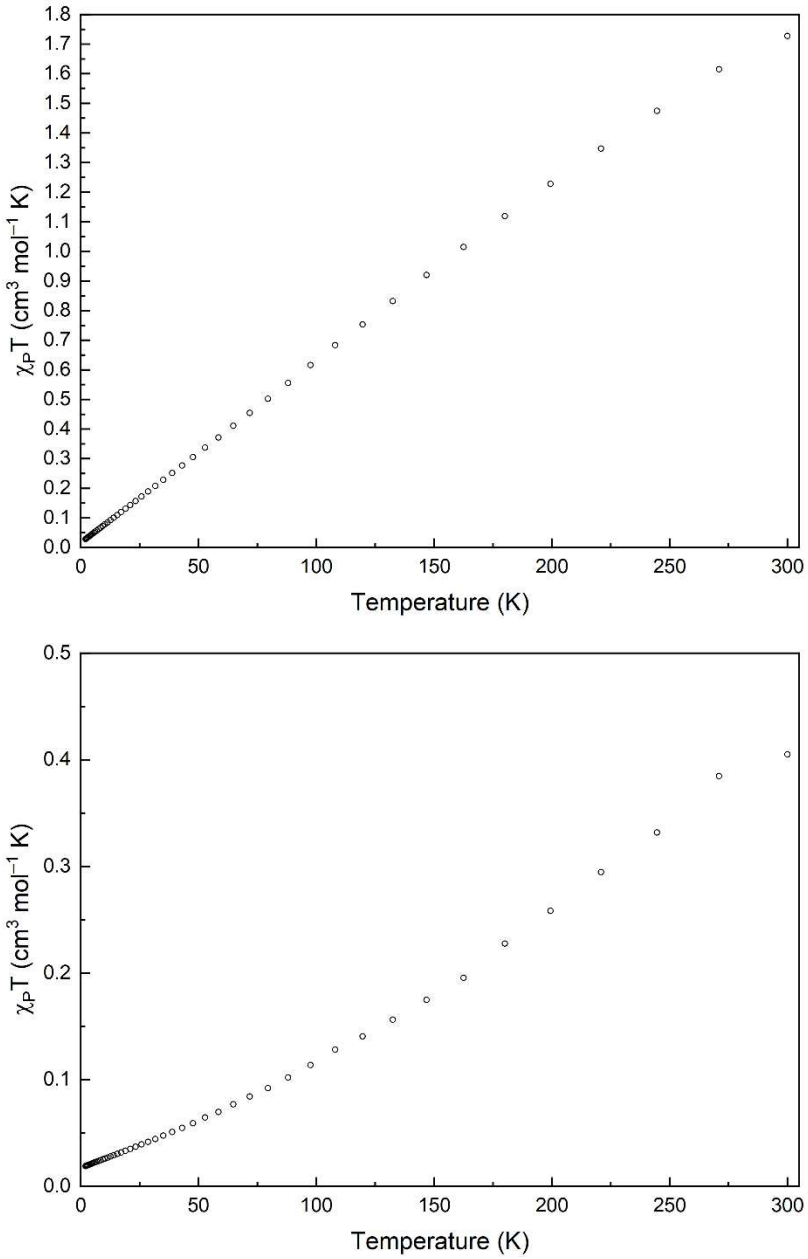

Figure S12. (Top) Uncorrected paramagnetic susceptibility data for **1a**$^{+}$**[Sb$_3$F$_{16}$]**$^{-}$**·1.5C$_6$F$_5$**; (bottom) paramagnetic susceptibility data corrected for inherent diamagnetism of the sample holder.

Comments: Because $\chi_P T$ = 0.019 cm^3 mol^{-1} K at 2 K (as opposed to the expected 0 cm^3 mol^{-1} K for the singlet system), it was necessary to model a $\vec{S} = 1/2$ paramagnetic impurity in the sample of 4.6%. This impurity arose from a small portion of the sample being oxidized, which was observed as a thin layer of pink powder on the top of the susceptibility sample. The non-linearity in the susceptibility data is due to imperfect correction of diamagnetism for the sample holder, since it was observed that the uncorrected data is completely linear (Figure S12).

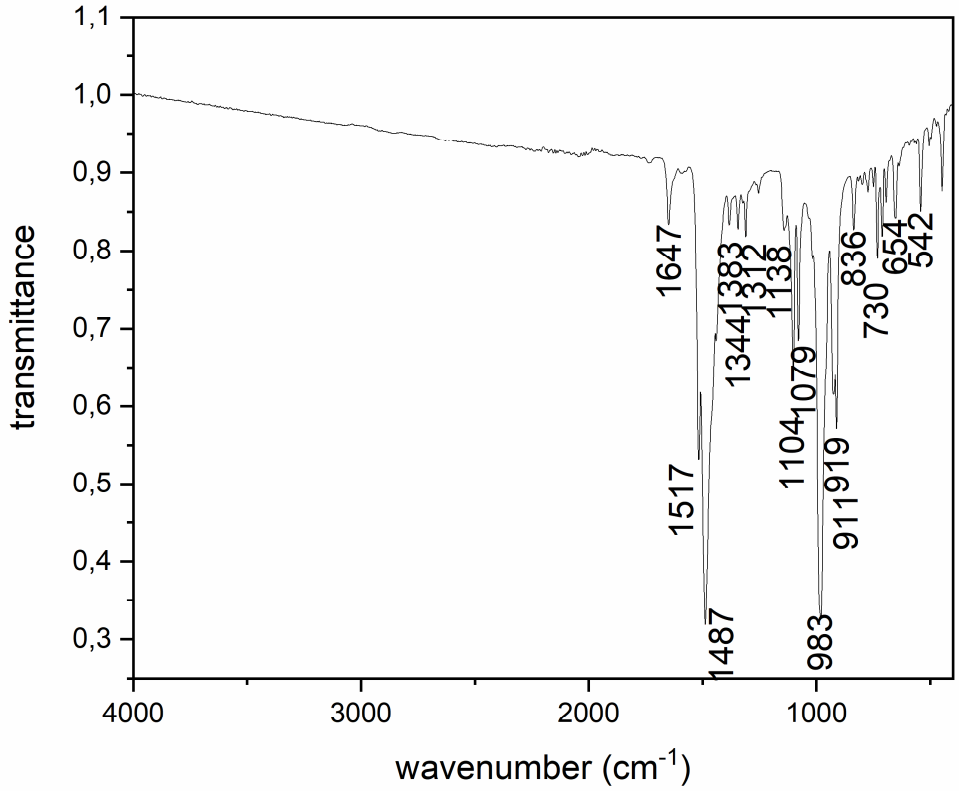

Figure S13. ATR-IR spectrum of the pentakis(pentafluorophenyl)cyclopentadienyl radical **2**.

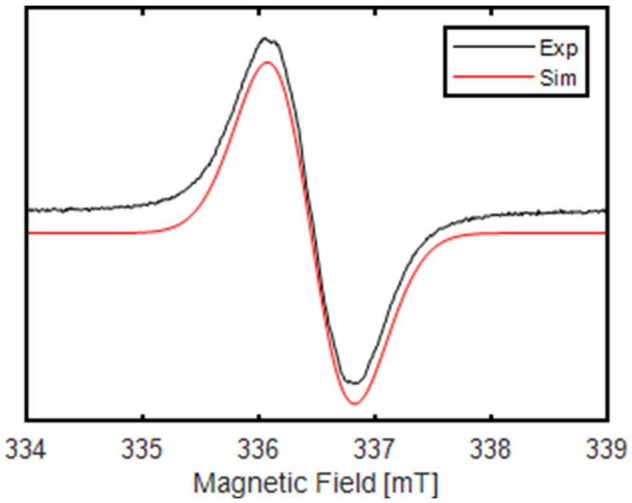

Figure S14. EPR spectrum of the pentakis(pentafluorophenyl)cyclopentadienyl radical **2**. For the simulation, a g value of 2.0033 and a linewidth (peak-to-peak) of 0.75 mT were used.

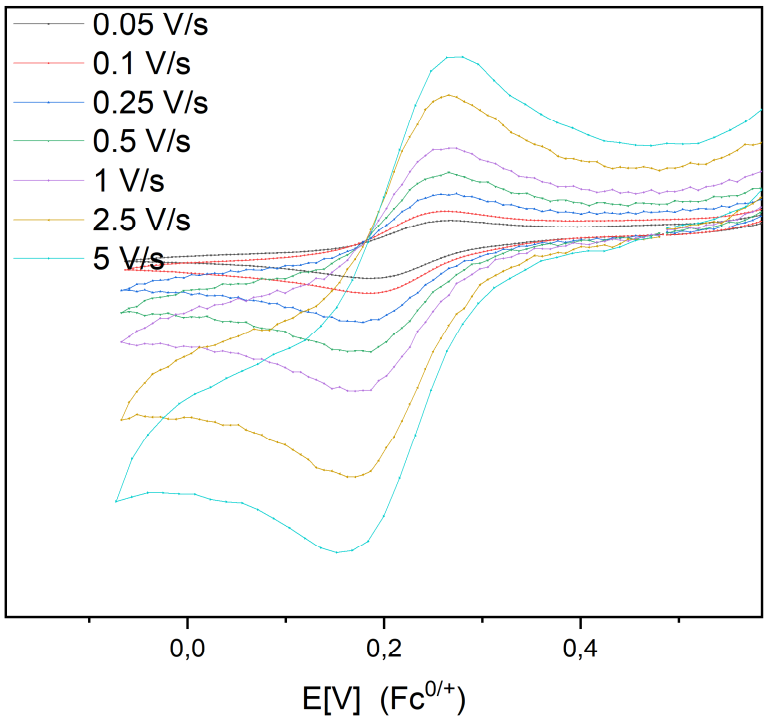

Figure S15. Cyclic voltammogramm of the pentakis(pentafluorophenyl)cyclopentadienyl radical **2** at 25 °C in 1,2-difluorobenzene. The reversible reduction to the corresponding anion **3** occurs at a half wave potential of $E_{1/2}$ = 0.48 V.

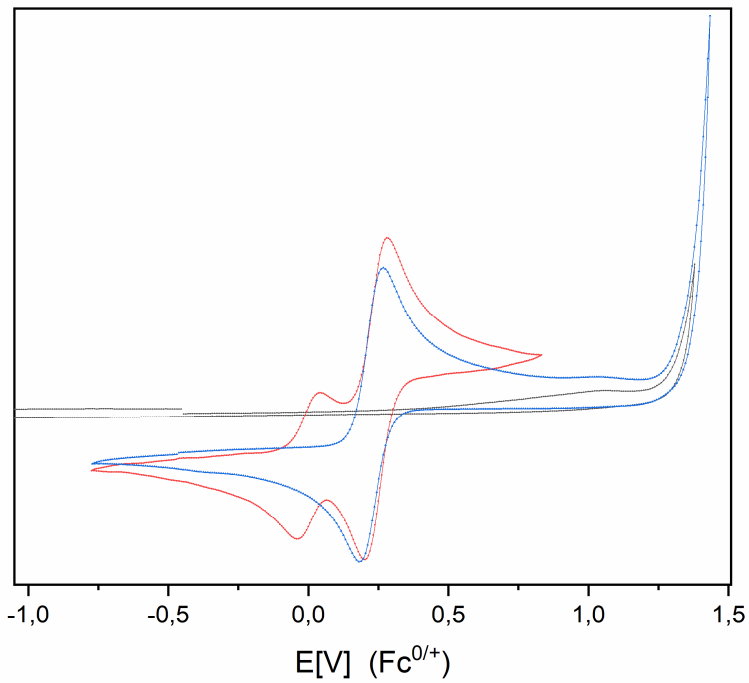

Figure S16. Cyclic voltammogramm of the pentakis(pentafluorophenyl)cyclopentadienyl radical **2** at 25 °C in 1,2-difluorobenzene. Black: only 1,2-difluorobenzene and $NBu_4B(Ph\text{-}3,5(CF_3)_2)_4$; blue: 1,2-difluorobenzene, $NBu_4B(Ph\text{-}3,5(CF_3)_2)_4$, and **2**; red: 1,2-difluorobenzene, $NBu_4B(Ph\text{-}3,5(CF_3)_2)_4$, **2** and ferrocene. No oxidation of **2** to **1** can be observed in the solvent window (up to 1.3 V).

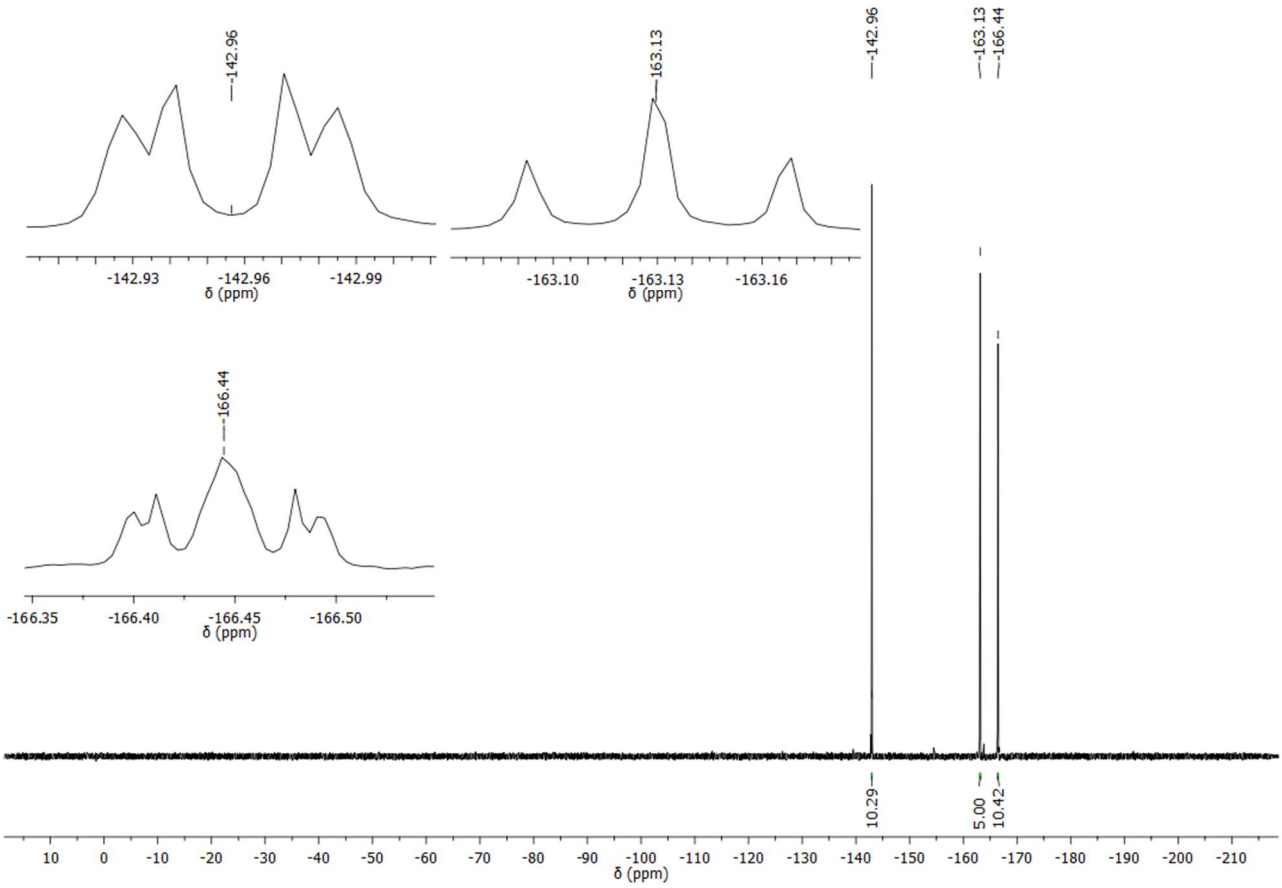

Figure S17. ^{19}F NMR spectrum of ferrocenium pentakis(pentafluorophenyl)cyclopentadienide **3a** in THF-d_8 at 25 °C.

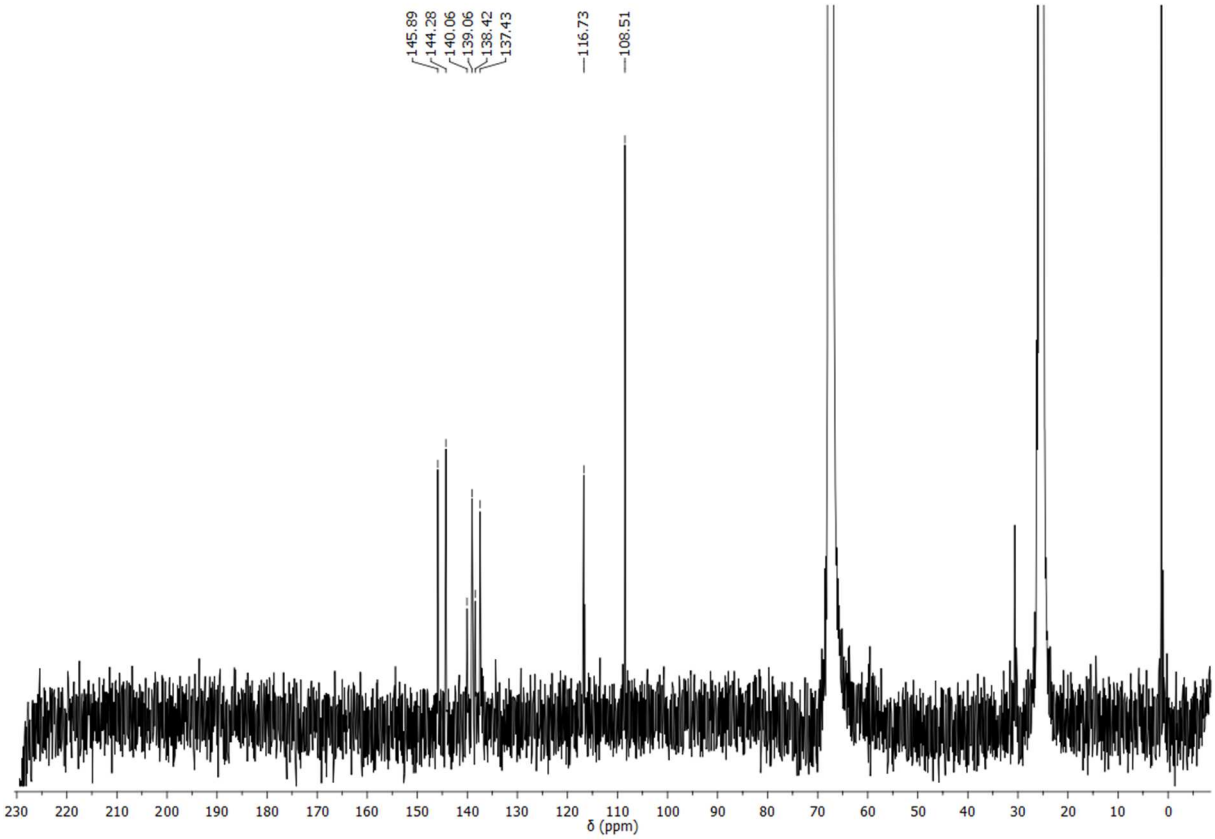

Figure S18. ^{13}C NMR spectrum of ferrocenium pentakis(pentafluorophenyl)cyclopentadienide **3a** in THF-d_8 at 25 °C.

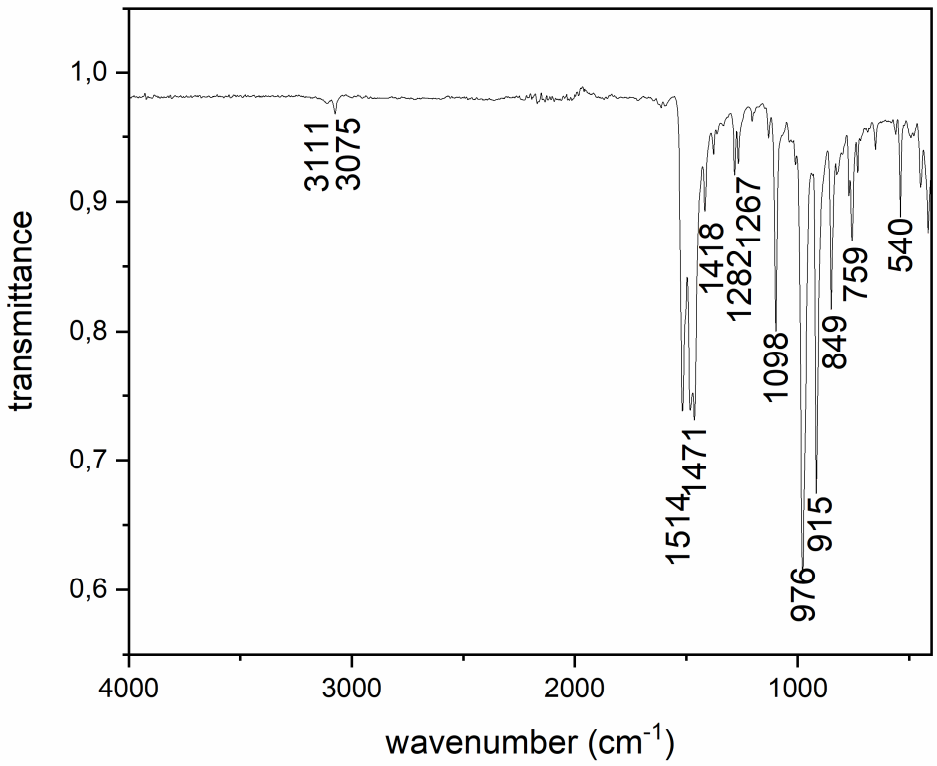

Figure S19. ATR-IR spectrum of ferrocenium pentakis(pentafluorophenyl)cyclopentadienide **3a**.

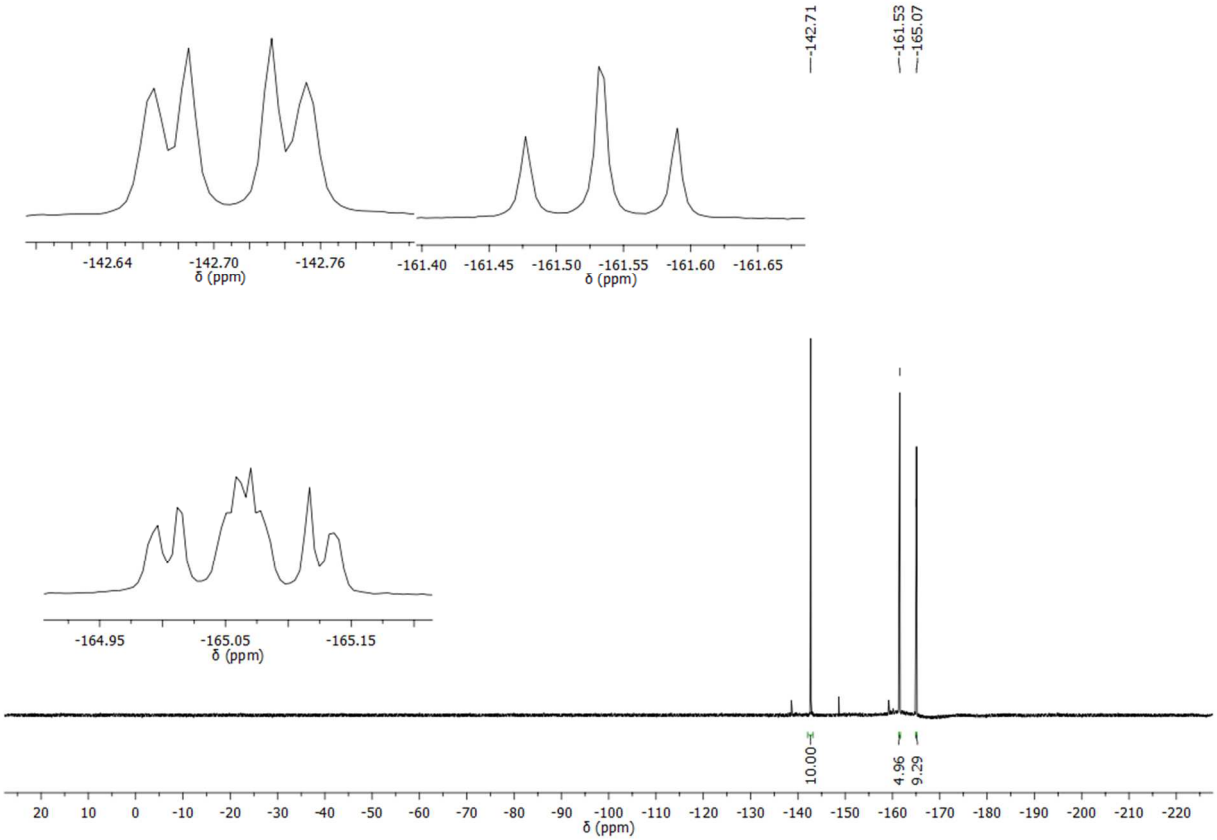

Figure S20. ^{19}F NMR spectrum of tritylium pentakis(pentafluorophenyl)cyclopentadienide **3b** in CD_2Cl_2 at 25 °C.

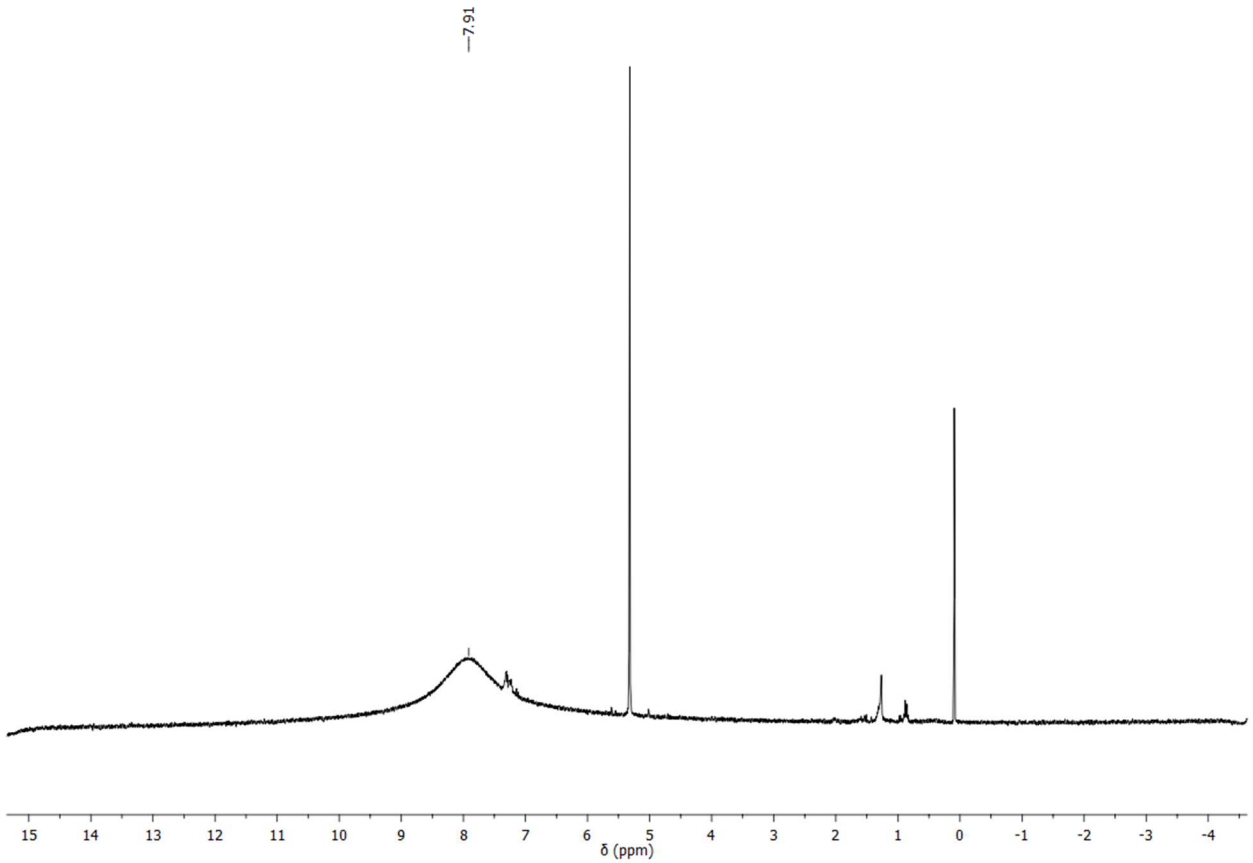

Figure S21. ^{1}H NMR spectrum of tritylium pentakis(pentafluorophenyl)cyclopentadienide **3b** in CD_2Cl_2 at 25 °C.

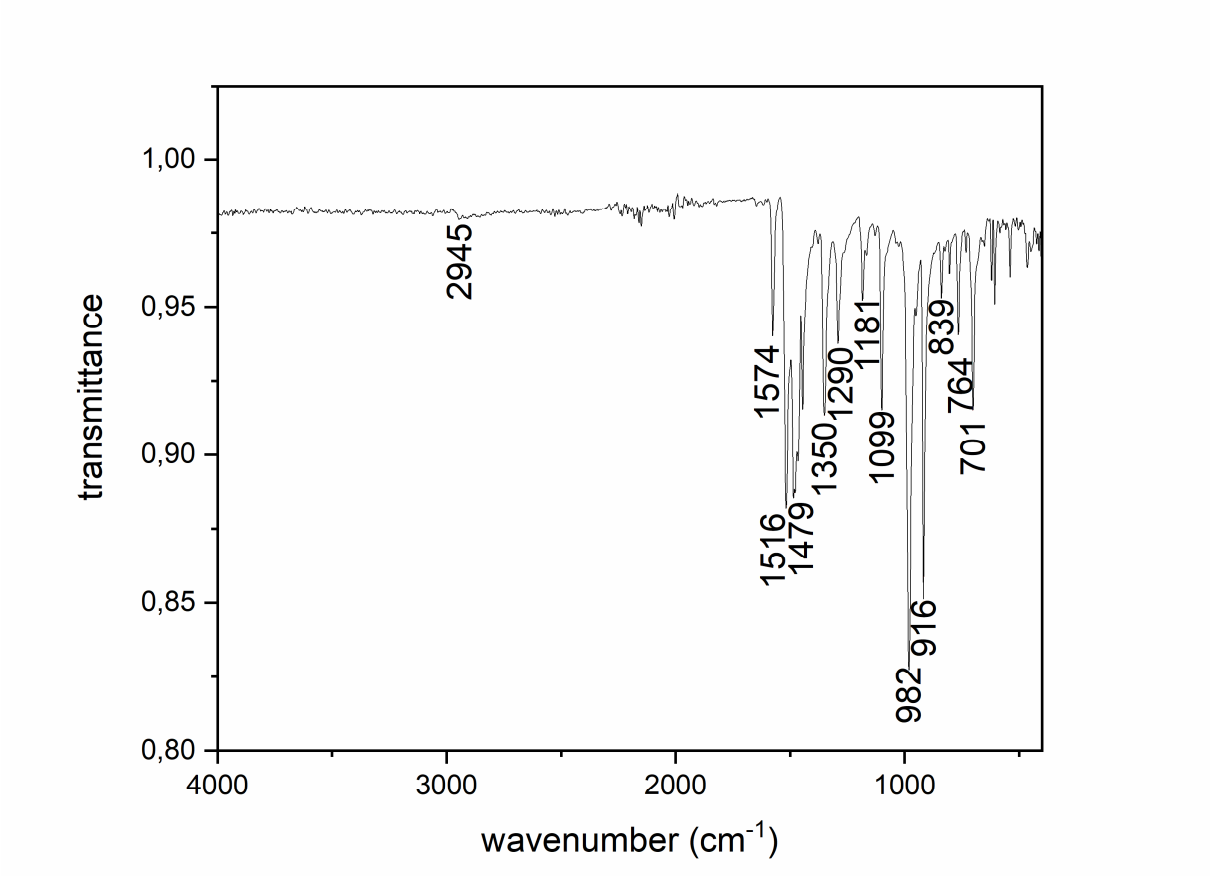

Figure S22. ATR-IR spectrum of tritylium pentakis(pentafluorophenyl)cyclopentadienide **3b**.

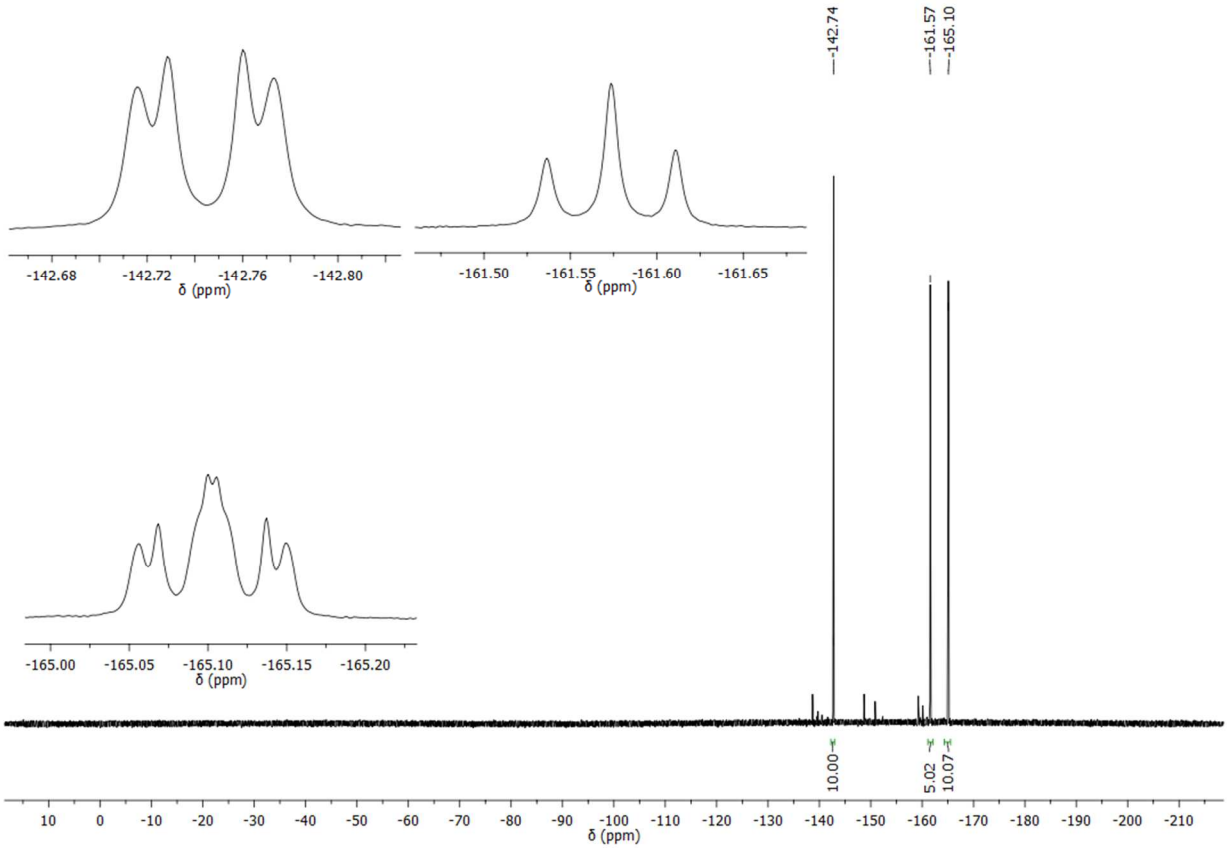

Figure S23. ^{19}F NMR spectrum of decamethylalumocenium pentakis(pentafluorophenyl)cyclopentadienide **3c** in CD_2Cl_2 at 25 °C.

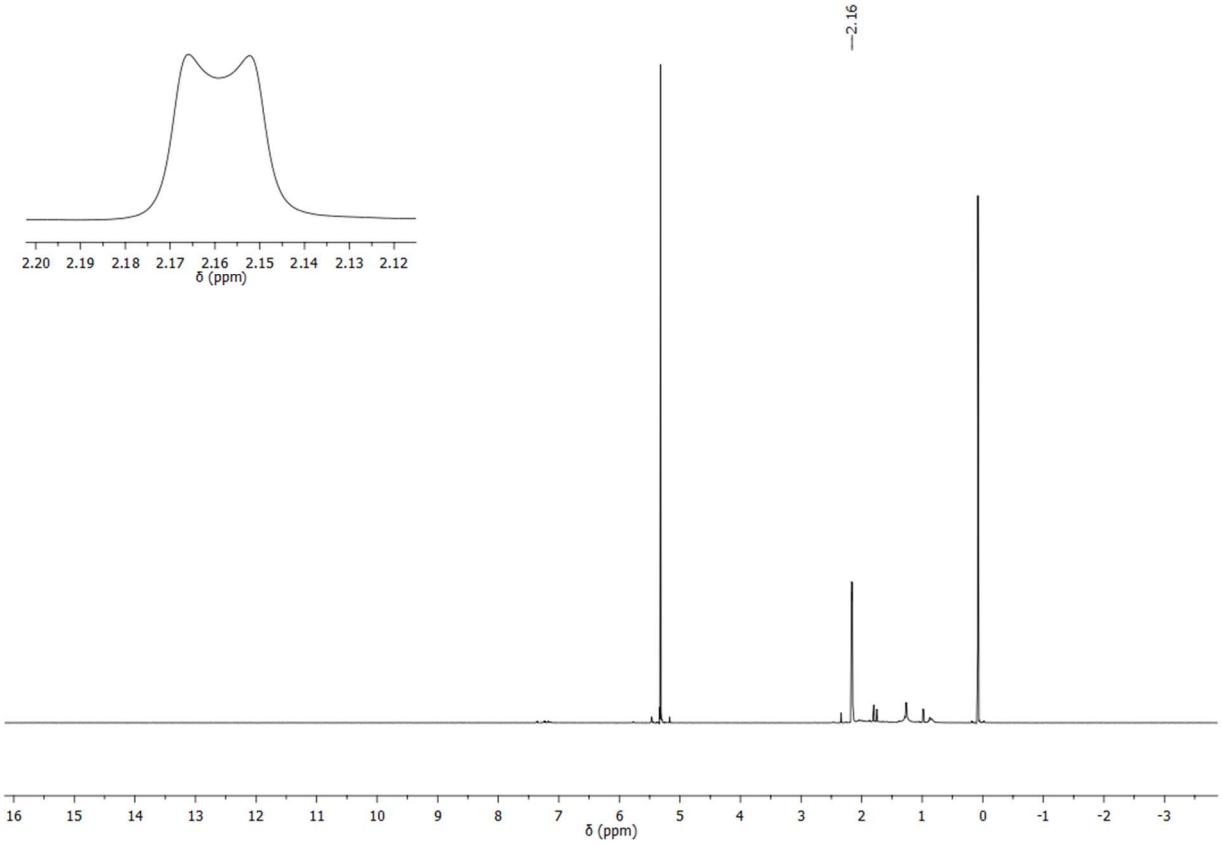

Figure S24. ^{1}H NMR spectrum of decamethylalumocenium pentakis(pentafluorophenyl)cyclopentadienide **3c** in CD_2Cl_2 at 25 °C.

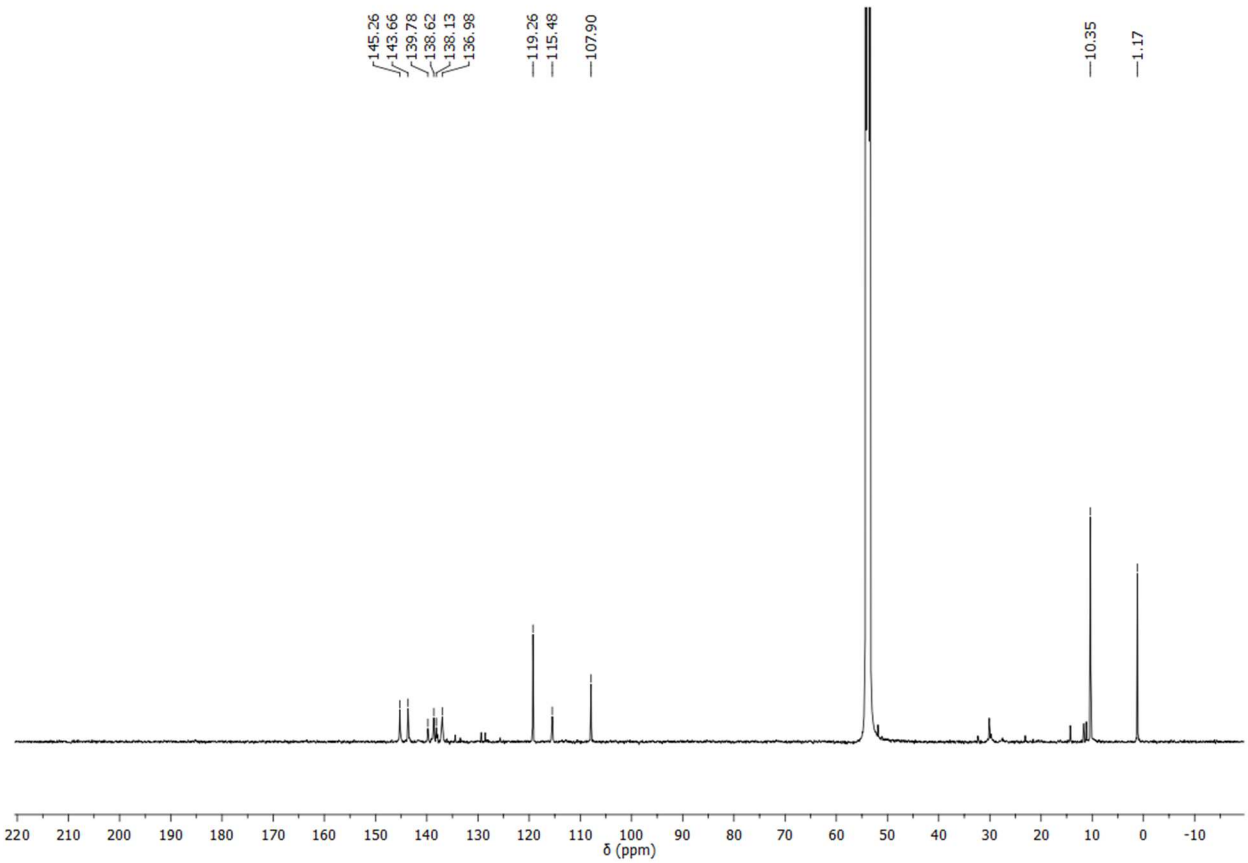

Figure S25. ^{13}C NMR spectrum of decamethylalumocenium pentakis(pentafluorophenyl)cyclopentadienide **3c** in CD_2Cl_2 at 25 °C.

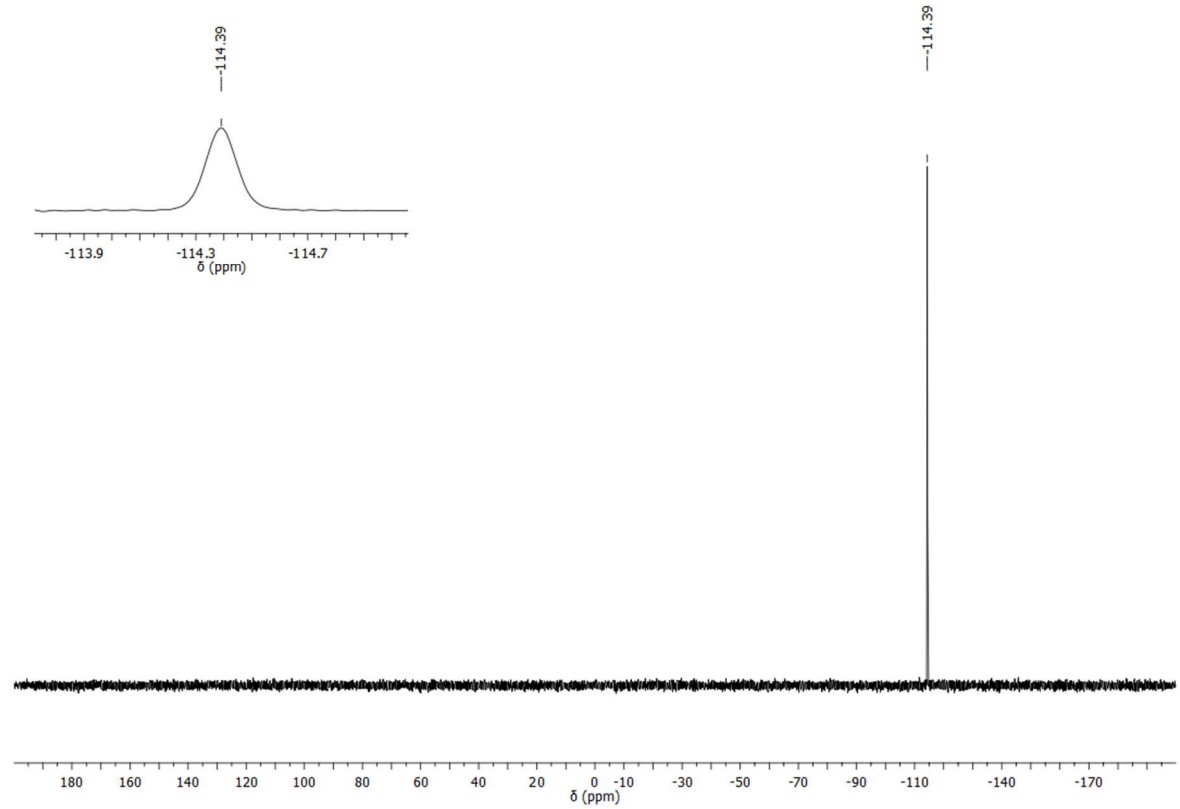

Figure S26. ^{27}Al NMR spectrum of decamethylalumocenium pentakis(pentafluorophenyl)cyclopentadienide **3c** in CD_2Cl_2 at 25 °C.

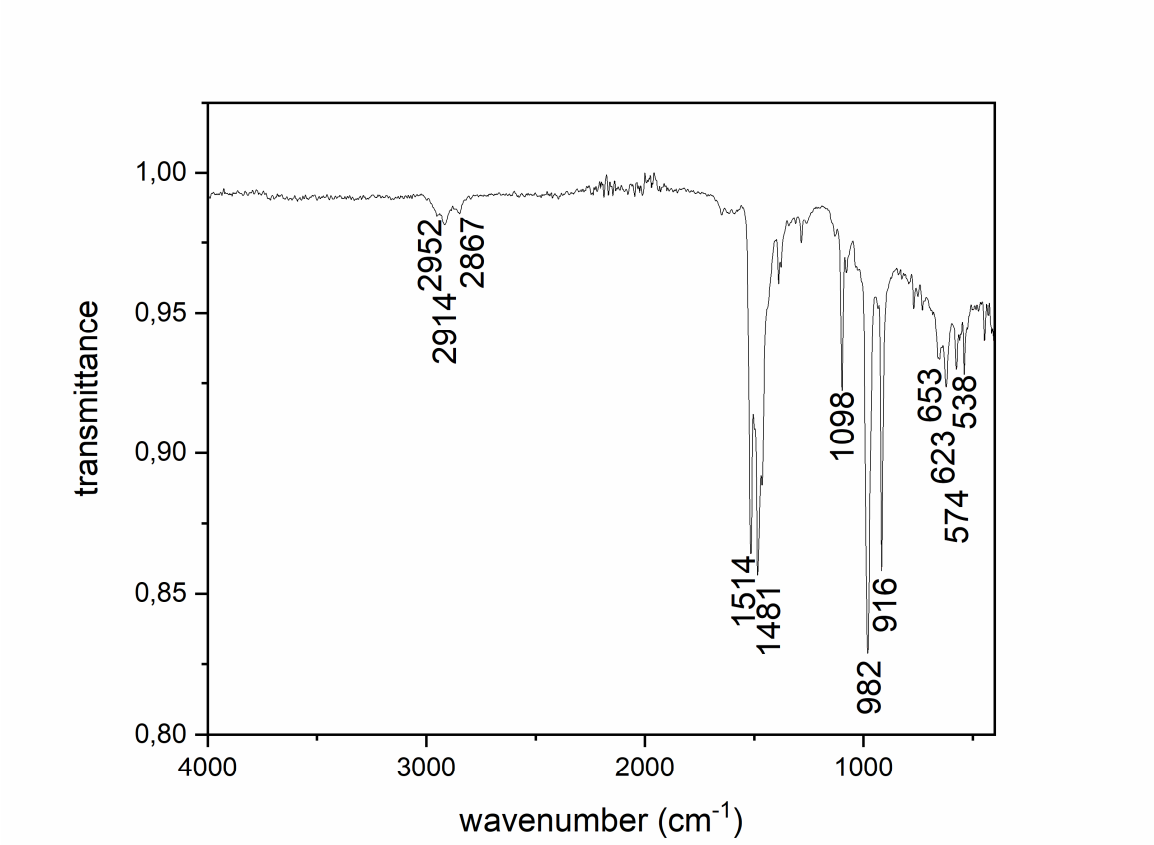

Figure S27. ATR-IR spectrum of decamethylalumocenium pentakis(pentafluorophenyl)cyclopentadienide **3c**.

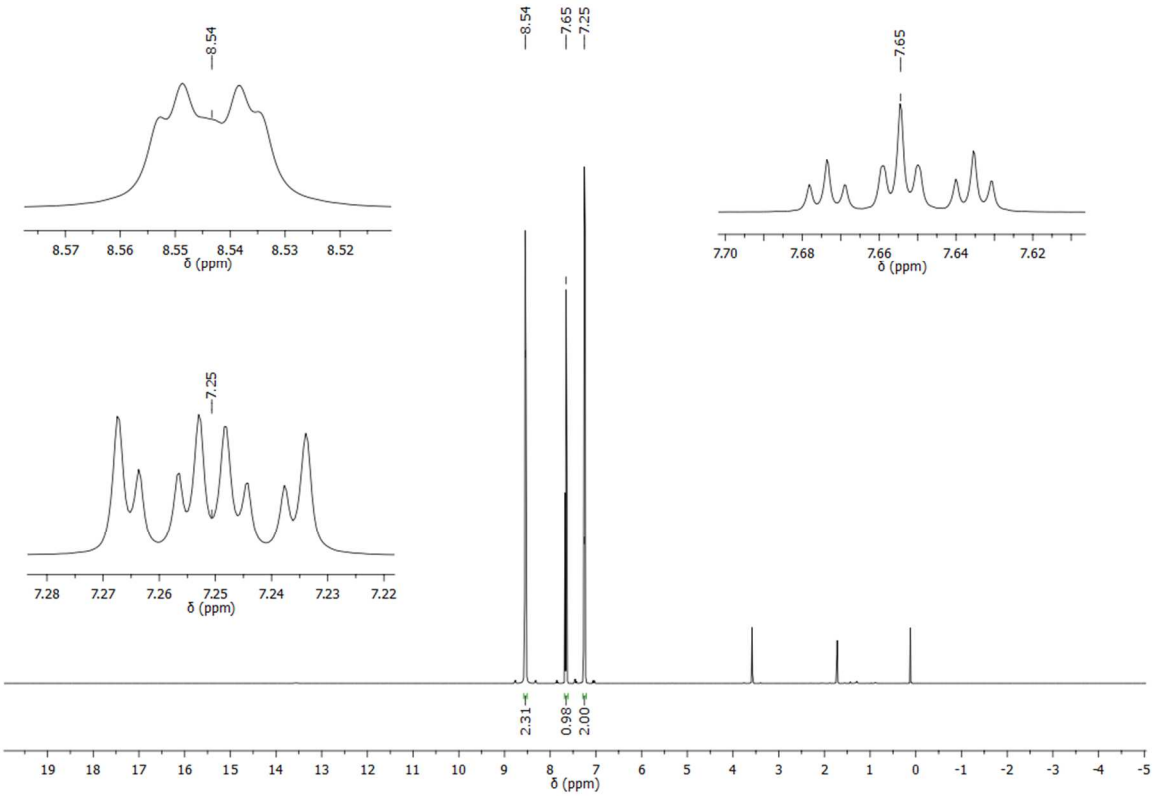

Figure S28. ^{1}H NMR spectrum of pyridinium pentakis(pentafluorophenyl)cyclopentadienide **3d** in thf-d_8 at 25 °C.

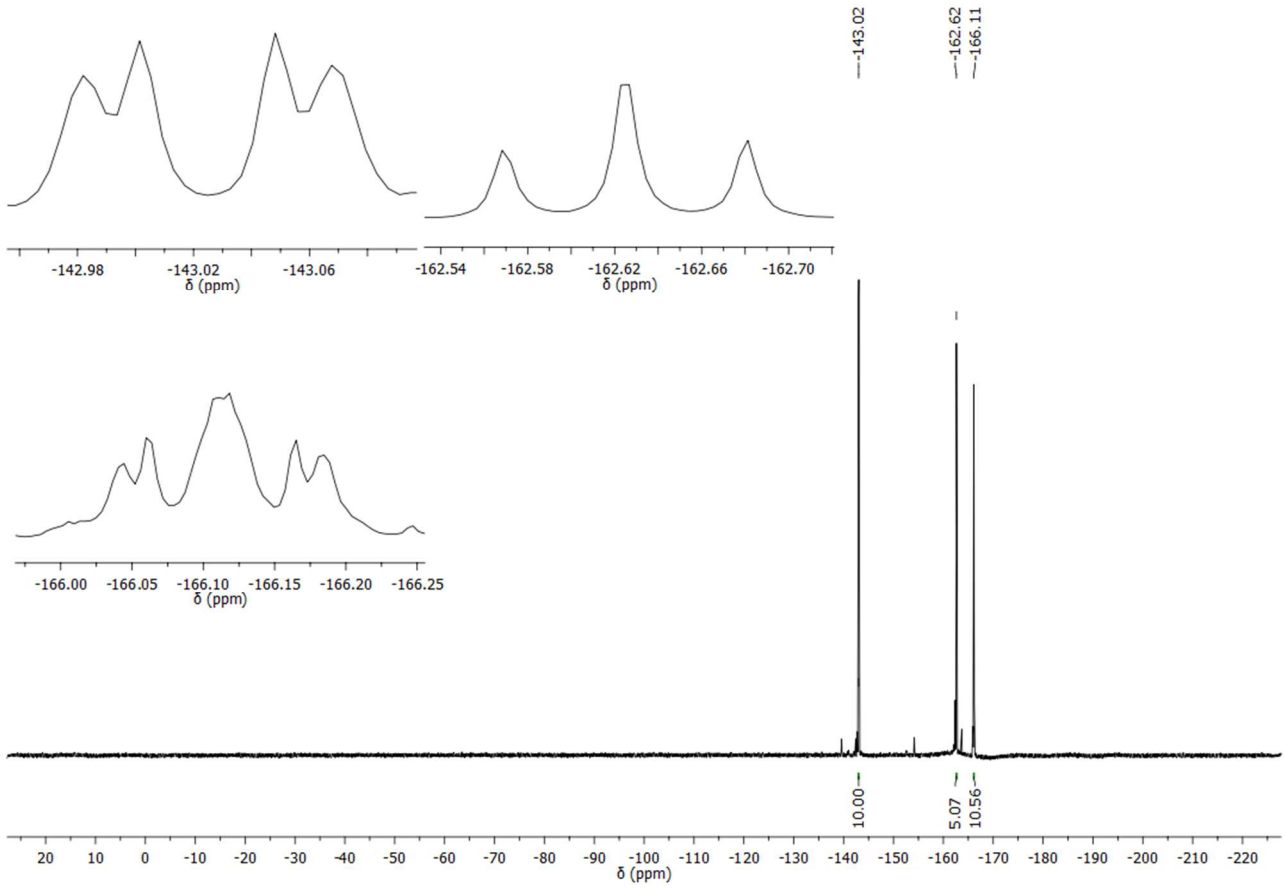

Figure S29. ^{19}F NMR spectrum of pyridinium pentakis(pentafluorophenyl)cyclopentadienide **3d** in thf-d_8 at 25 °C.

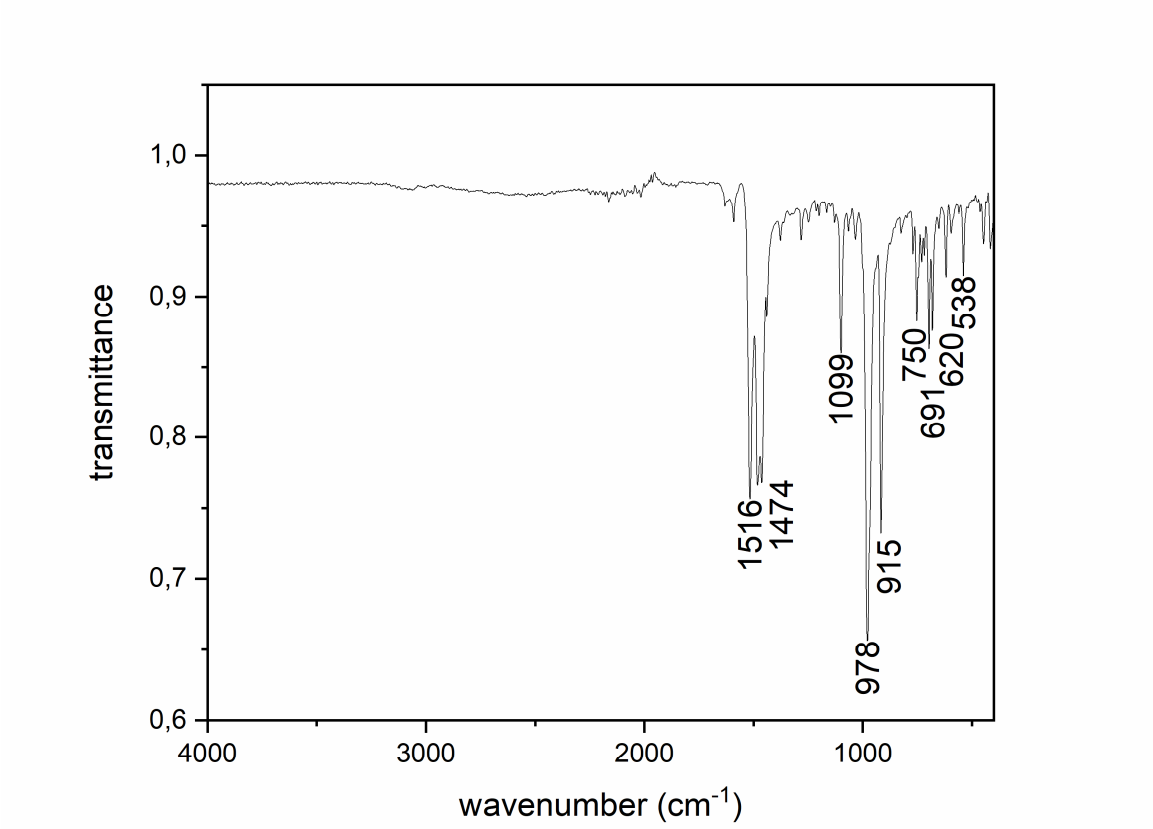

Figure S30. ATR-IR spectrum of pyridinium pentakis(pentafluorophenyl)cyclopentadienide **3d**.

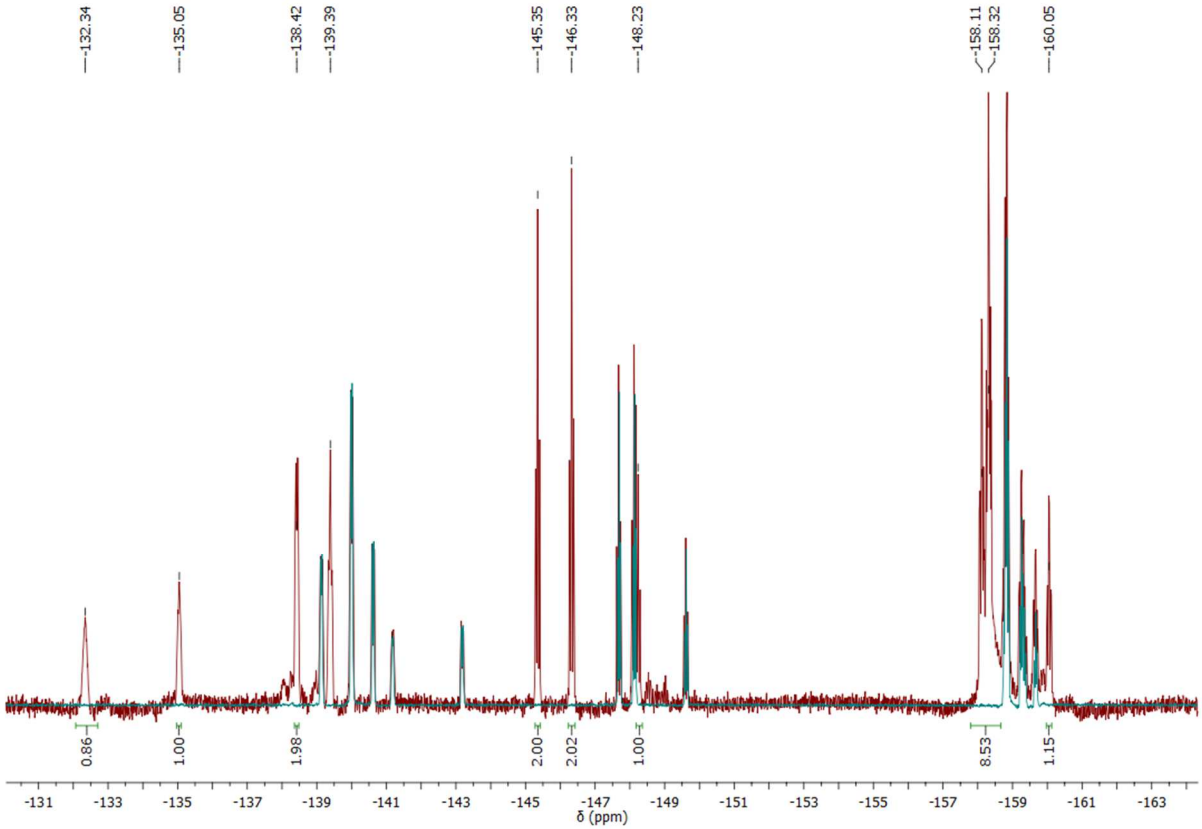

Figure S31. ^{19}F NMR spectrum of pentakis(pentafluorophenyl)cyclopentadienyl carboxylic acid **5** and pentakis(pentafluorophenyl)cyclopentadiene **6** (red) and pure pentakis(pentafluorophenyl)cyclopentadiene **6** (cyan) in C_6D_6 at 25 °C.

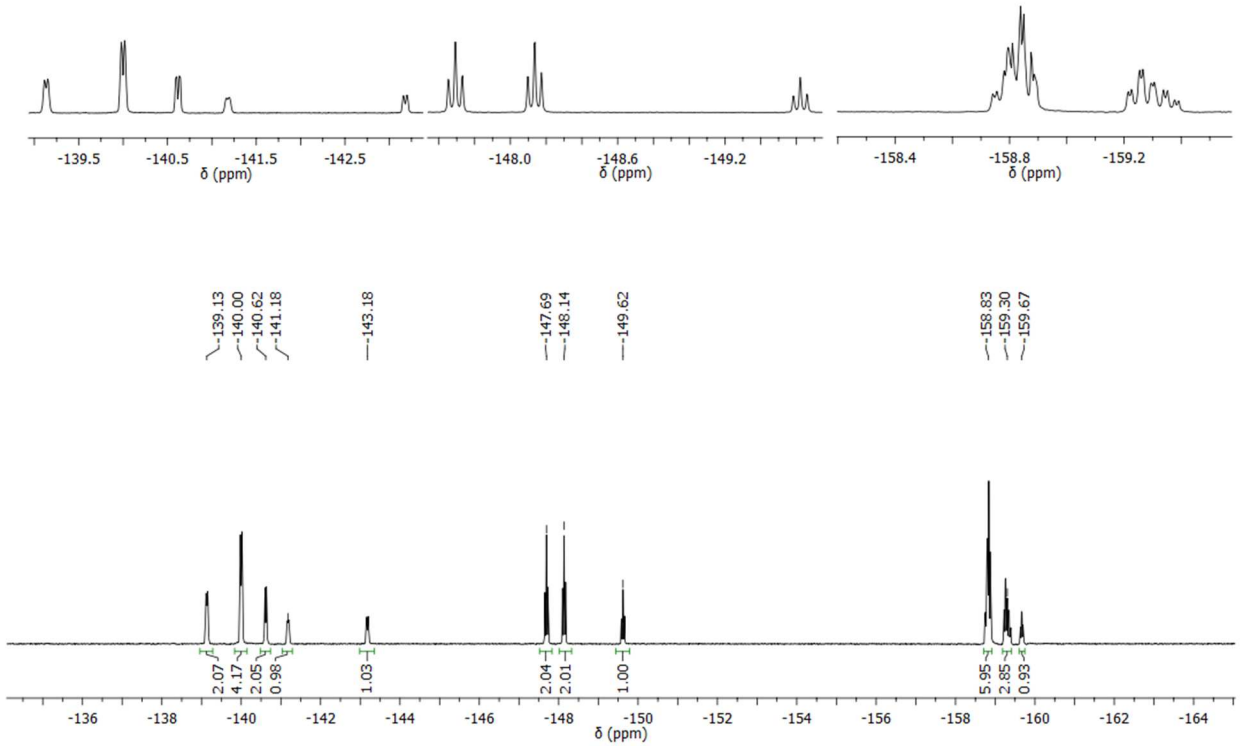

Figure S32. ^{19}F NMR spectrum of pentakis(pentafluorophenyl)cyclopentadiene **6** in C_6D_6 at 25 °C.

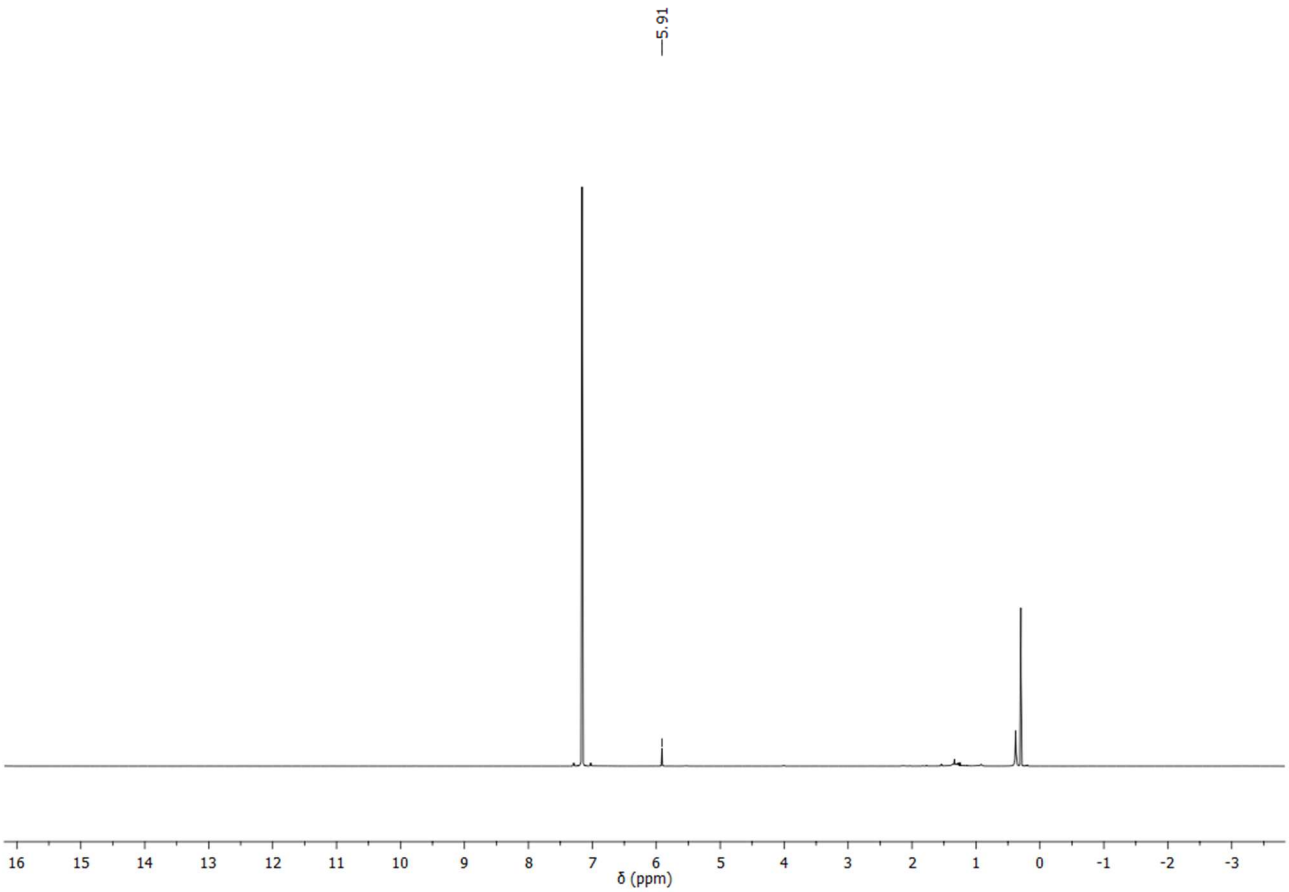

Figure S33. ^{1}H NMR spectrum of pentakis(pentafluorophenyl)cyclopentadiene **6** in C_6D_6 at 25 °C.

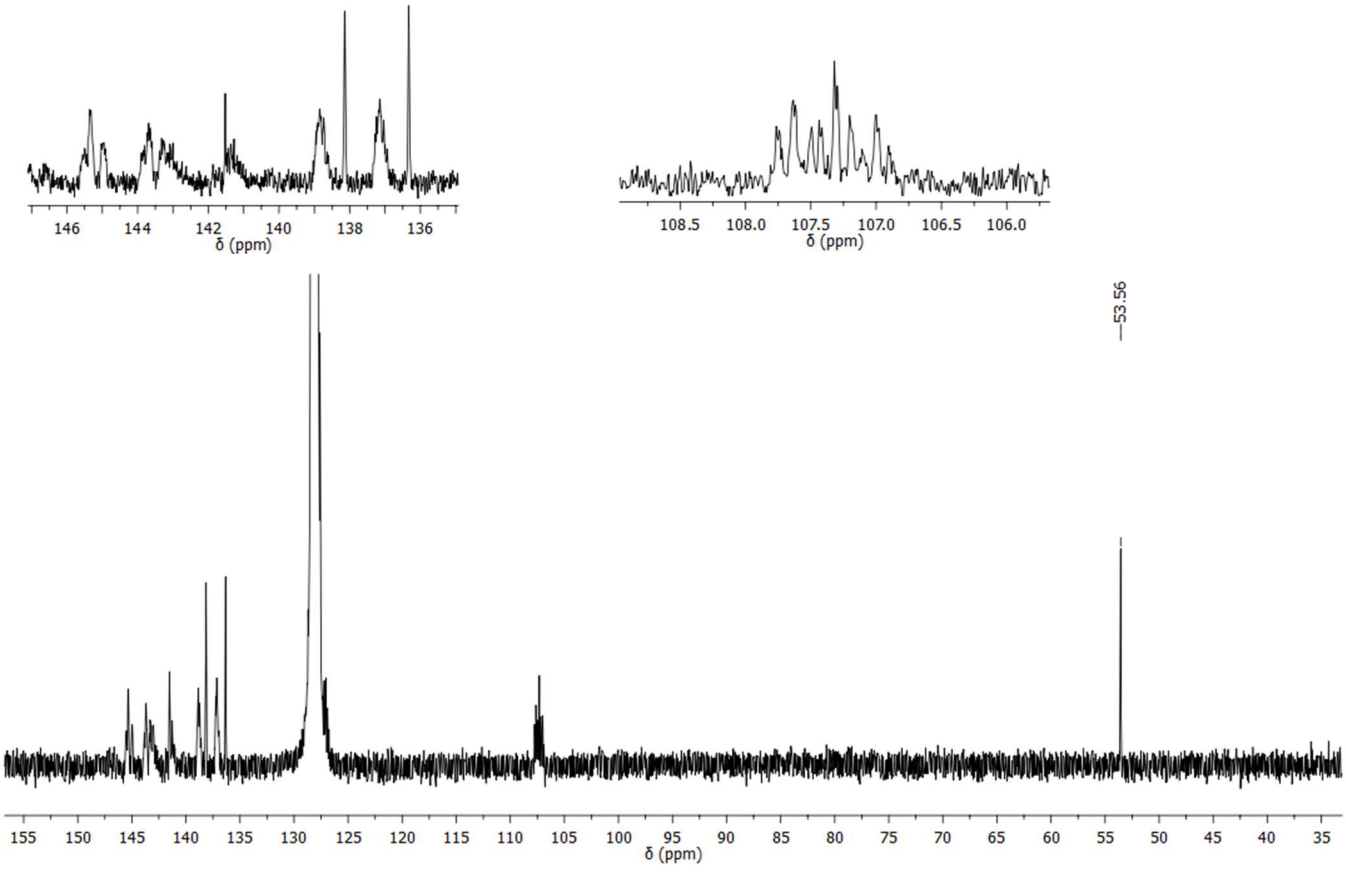

Figure S34. ^{13}C{^{1}H} NMR spectrum of pentakis(pentafluorophenyl)cyclopentadiene **6** in C_6D_6 at 25 °C.

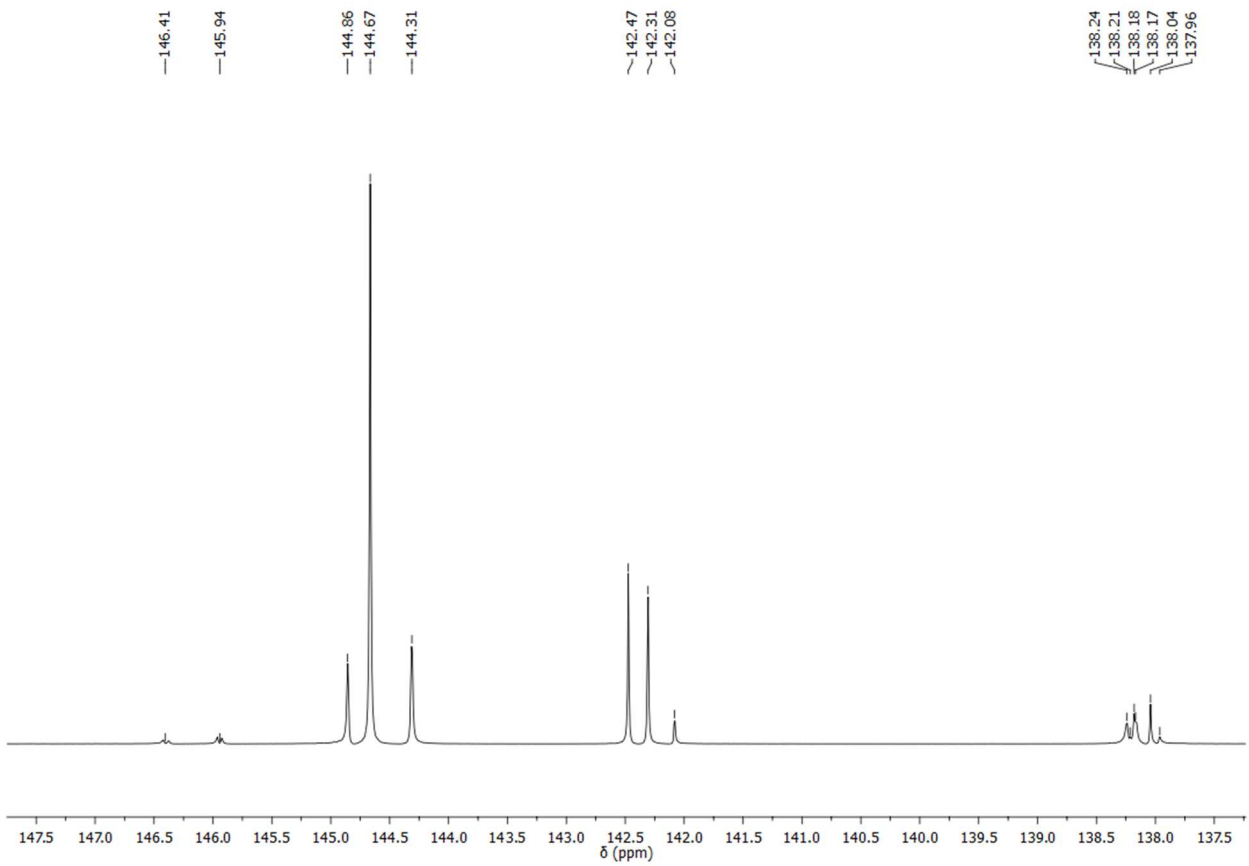

Figure S35. $^{13}C\{^{1}H\}$ DEPT-135 NMR spectrum of pentakis(pentafluorophenyl)cyclopentadiene **6** in C_6D_6 at 25 °C.

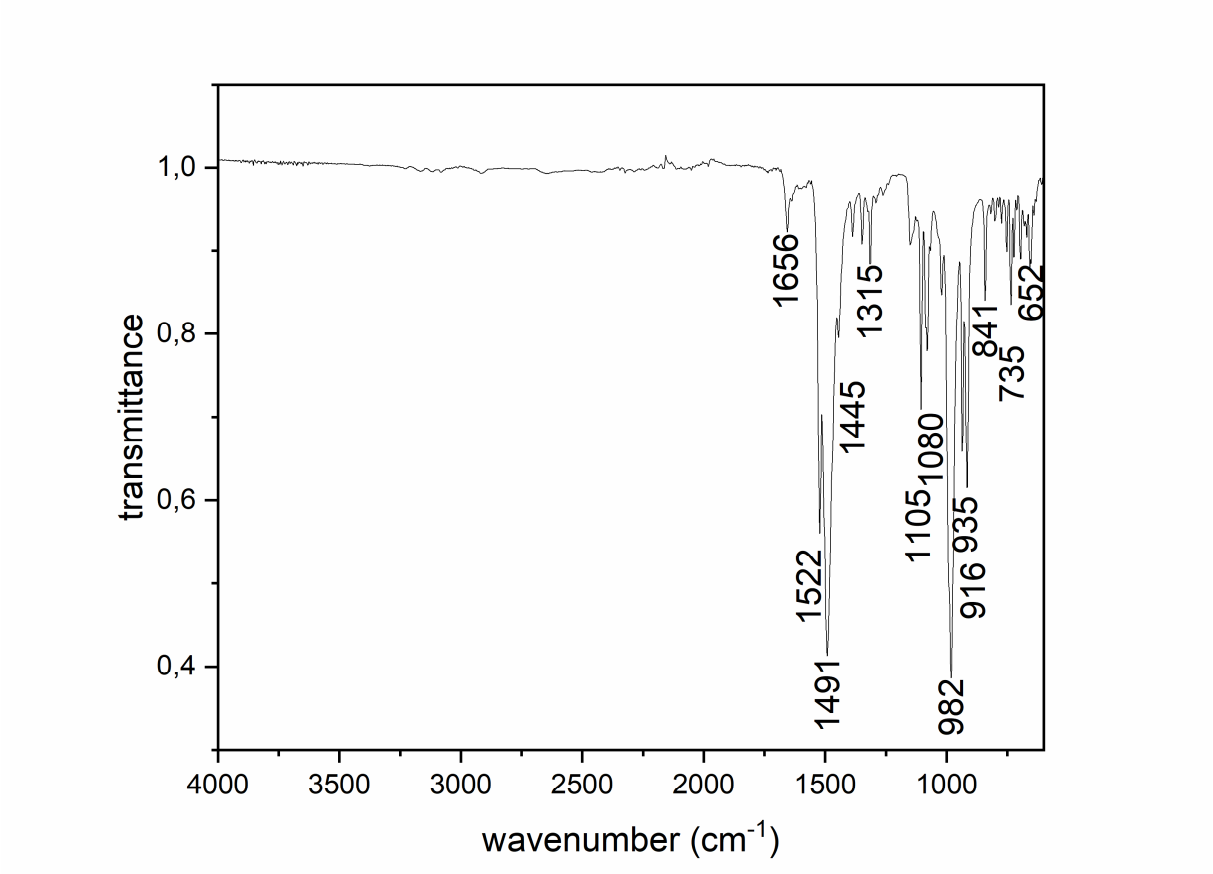

Figure S36. ATR-IR spectrum of pentakis(pentafluorophenyl)cyclopentadiene **6**.

III. Crystallographic Data

Single-crystal X-ray analyses. Crystals were mounted on nylon loops in inert oil. Data of $\mathbf{1b^+[Sb_3F_{16}]^-\cdot 1C_6F_6}$ were collected on a Bruker AXS D8 Kappa diffractometer with APEX2 detector (monochromated $Mo_{K\alpha}$ radiation, λ = 0.71073 Å) at 100(2) K. Data of **B**, $\mathbf{C_6(C_6F_5)_6}$, $\mathbf{1a^+[Sb_3F_{16}]^-\cdot 1.5C_6F_6}$, **2a**, **2b**, **3a**, **3b**, **3c**, **5**, and **6** were collected on a Bruker AXS D8 Venture diffractometer with Photon II detector (monochromated $Cu_{K\alpha}$ radiation, λ = 1.54178 Å, microfocus source) at 100(2) K. The structures were solved by Direct Methods (SHELXS-2013)[7] and refined anisotropically by full-matrix least-squares on F^2 (SHELXL-2017)[8,9]. Absorption corrections were performed semi-empirically from equivalent reflections on basis of multi-scans or numerical from indexed faces (**1b**) (Bruker AXS APEX3). Hydrogen atoms were refined using a riding model or rigid methyl groups. In $\mathbf{C_6(C_6F_5)_6}$ a $-C_6F_5$ is disordered over two positions. The bond lengths and angles of the phenyl ring were restrained to be equal (SADI). SIMU and RIGU restraints were applied to the displacement parameters of the group. The displacement parameters of the carbon atoms were constrained to be equal for the alternate positions (EADP). In $\mathbf{1a^+[Sb_3F_{16}]^-\cdot 1.5C_6F_6}$ one solvent molecule is disordered over a center of inversion. The local symmetry was ignored in the refinement and the C–C bond lengths and angles of the solvent molecule were restrained to be equal as well as the F/F distances (SADI). RIGU restraints were applied to the displacement parameters of the solvent molecules' atoms. The only available specimen of **1b** was too large for the X-ray beam and we did not want to risk losing it by trying to cut it. Any attempts to obtain a more suitable one yielded the other polymorph. The uneven irradiation of the crystal led to distortions of the reflection intensities and consequently to problems with the absorption correction. Several methods and setting were tried but the residual electron density could not be reduced any further. Quantitative results should be carefully assessed. The solvent molecule is disordered over two positions. Its C–C bond lengths and C–C–C bond angles were restrained to be equal (SADI) as well as the F/F distances. All atoms of the molecule were restrained to lie on a common plane (FLAT). The crystal of **2a** was a non-merohedral twin and the model was refined against de-twinned HKLF4 data. Due to overlaps, the R_{int} value is rather high. One of the SO_2 molecules in **2b** is disordered over two alternate sites. The bond lengths and angles of the SO_2 molecules were restrained to be equal (SADI), and RIGU restraints were applied to their displacement parameters. The residual electron density suggests that two of the C_6F_5 rings may be disordered, however a refinement failed due to the low occupancy. **3a** was refined as an inversion twin. In **3b** a C_6F_5 is disordered over two positions. SIMU and RIGU restraints were applied to the displacement parameters of the corresponding atoms. Due to their close proximity F35 and F35' were refined with common displacement parameters (EADP). The structure also contains highly disordered solvent – possibly toluene. The final refinement was done with a solvent free dataset from a PLATON/SQUEEZE run.[10] Since the nature and amount of the solvent is not clear it was not included in the sum formula. The quality of the diffraction data of **3c** was rather low (high *Rint*). To check the correct assignment of the Laue group the frames were integrated with a triclinic unit cell. This lead to an equally poor R_{int}. Considering the low quality of the data quantitative results should be carefully assessed. The hydrogen atom of **5** was refined freely. The structure contains highly disordered solvent molecules: one hexafluoro benzene and two *n*-hexane disordered over special positions (2, -1 and 222). The final refinement was done with a solvent free data set from a PLATON/SQUEEZE run.[10] The molecules were included in the sum formula for completeness. The quality of the best specimen available was still rather poor and consequently results beyond the connectivity may be unreliable and should be carefully assessed.

Table S1. Crystal and structure refinement data of **B**, **$C_6(C_6F_5)_6$**, **$1a^+$**, **$1b^+$**, **2a–b**, **3a–c**, **5**, and **6**.

Identification code	**B**	**$C_6(C_6F_5)_6$**	**2a**	**3a**
Empirical formula	$C_{14}F_{10}$	$C_{42}F_{30}$	$C_{35}F_{25}$	$C_{51}H_{14}F_{27}Fe$
M	358.14	1074.42	895.35	1195.47
Crystal size [mm]	0.541 × 0.461 × 0.072	0.252 × 0.136 × 0.074	0.211 × 0.062 × 0.036	0.258 × 0.068 × 0.049
T [K]	100(2)	100(2)	100(2)	100(2)
Crystal system	monoclinic	orthorhombic	monoclinic	monoclinic
Space group	*C*2/*m*	*Pna*2$_1$	*C*2/*c*	*Cc*
a [Å]	8.9583(11)	12.8398(12)	22.3002(17)	10.7524(4)
b [Å]	7.6581(10)	22.205(2)	13.5353(11)	20.8342(7)
c [Å]	9.2374(12)	13.0139(11)	11.4185(9)	20.0712(7)
α [°]	90	90	90	90
β [°]	110.222(3)	90	116.061(3)	96.603(2)
γ [°]	90	90	90	90
V [Å^3]	594.65(13)	3710.3(6)	3096.1(4)	4466.5(3)
Z	2	4	4	4
D_{calc} [g·cm^{-3}]	2.000	1.923	1.921	1.778
μ(CuK_α [mm^{-1}])	2.098	2.018	2.015	4.123
Transmissions	0.75/0.44	0.75/0.58	0.75/0.47	0.75/0.53
F(000)	348	2088	1740	2356
Index ranges	$-11 \le h \le 9$	$-16 \le h \le 16$	$-28 \le h \le 25$	$-13 \le h \le 10$
	$-9 \le k \le 9$	$-22 \le k \le 28$	$0 \le k \le 17$	$-26 \le k \le 26$
	$-11 \le l \le 11$	$-16 \le l \le 16$	$0 \le l \le 14$	$-25 \le l \le 25$
θ_{max} [°]	79.642	80.740	80.306	81.190
Reflections collected	9187	80749	53232	65031
Independent reflections	699	7972	3359	8679
R_{int}	0.0491	0.0462	0.1450	0.0976
Refined parameters	61	713	273	713
R_1 [$I > 2\sigma(I)$]	0.0398	0.0277	0.0619	0.0360
wR_2 [all data]	0.1368	0.0737	0.1543	0.0799
x(Flack)	–	0.00(2)	–	0.362(5)
GooF	1.240	1.039	1.090	1.040
$\Delta\rho_{final}$ (max/min) [e·Å^{-3}]	0.262/-0.304	0.322/-0.152	0.320/-0.243	0.269/-0.393

Table S1. Crystal and structure refinement data (continuation).

Identification code	2b	3b	3c	6
Empirical formula	$C_{35}F_{25}O_4S_2$	$C_{54}H_{15}F_{25}$	$C_{55}H_{30}Al\ F_{25}$	$C_{35}HF_{25}$
M	1023.47	1138.66	1192.77	896.36
Crystal size [mm]	0.390 × 0.172 × 0.070	0.345 × 0.183 × 0.092	0.162 × 0.064 × 0.055	0.152 × 0.116 × 0.083
T [K]	100(2)	100(2)	100(2)	100(2)
Crystal system	triclinic	monoclinic	monoclinic	triclinic
Space group	P-1	$P2_1/c$	$P2_1/c$	P-1
a [Å]	11.1864(13)	14.2425(7)	15.6538(10)	12.7006(9)
b [Å]	11.3372(10)	20.3955(10)	14.8935(9)	13.3258(8)
c [Å]	16.478(3)	20.0632(10)	21.2611(14)	18.1289(17)
α [°]	106.938(9)	90	90	91.743(6)
β [°]	91.037(10)	99.626(3)	101.546(4)	95.967(6)
γ [°]	117.347(8)	90	90	90.570(5)
V [Å^3]	1747.1(4)	5746.0(5)	4856.5(5)	3049.9(4)
Z	2	4	4	4
D_{calc} [g·cm^{-3}]	1.946	1.316	1.631	1.952
μ(CuK_α [mm^{-1}])	3.063	1.205	1.617	2.046
Transmissions	0.75/0.51	0.75/0.54	0.75/0.59	0.75/0.63
F(000)	998	2256	2392	1744
Index ranges	$-14 \le h \le 12$	$-17 \le h \le 12$	$-19 \le h \le 19$	$-16 \le h \le 14$
	$-14 \le k \le 14$	$-26 \le k \le 25$	$-18 \le k \le 18$	$-17 \le k \le 17$
	$-20 \le l \le 20$	$-25 \le l \le 25$	$-23 \le l \le 26$	$-22 \le l \le 23$
θ_{max} [°]	75.114	81.806	80.572	81.119
Reflections collected	94339	134589	196985	169427
Independent reflections	7163	12546	10504	13260
R_{int}	0.0509	0.0788	0.1482	0.0485
Refined parameters	623	806	740	1081
R_1 [$I > 2\sigma(I)$]	0.0550	0.0672	0.0540	0.0366
wR_2 [all data]	0.1684	0.1670	0.1485	0.0987
GooF	1.049	1.095	1.026	1.017
$\Delta\rho_{final}$ (max/min) [e·Å^{-3}]	0.754/-0.480	0.446/-0.253	0.466/-0.392	0.533/-0.271

Table S1. Crystal and structure refinement data (continuation).

Identification code	**1b$^+$[Sb$_3$F$_{16}$]$^-$·1C$_6$F$_6$)**	**1a$^+$[Sb$_3$F$_{16}$]$^-$·1.5C$_6$F$_6$)**	**5**
Empirical formula	$C_{47}F_{53}Sb_3$	$C_{44}F_{50}Sb_3$	$C_{43.50}H_{11.50}F_{28}O_2$
M	1936.72	1843.69	1098.03
Crystal size [mm]	1.008 × 0.255 × 0.212	0.213 × 0.138 × 0.073	0.380 × 0.125 × 0.100
T [K]	100(2)	100(2)	100(2)
Crystal system	orthorhombic	monoclinic	orthorhombic
Space group	$Pna2_1$	$P2_1/c$	$Fddd$
a [Å]	27.1610(13)	23.1788(8)	11.6321(6)
b [Å]	15.5739(8)	10.9694(4)	47.785(2)
c [Å]	13.0018(6)	22.1030(8)	60.097(3)
α [°]	90	90	90
β [°]	90	113.0712(15)	90
γ [°]	90	90	90
V [Å^3]	5499.8(5)	5170.4(3)	33405(3)
Z	4	4	32
D_{calc} [g·cm^{-3}]	2.339	2.369	1.747
μ(CuK_α [mm^{-1}])	1.682 (MoK_α)	14.417	1.769
Transmissions	0.27/0.16	0.49/0.12	0.75/0.57
F(000)	3648	3468	17296
Index ranges	$-45 \le h \le 45$	$-29 \le h \le 29$	$-14 \le h \le 14$
	$-26 \le k \le 26$	$-13 \le k \le 14$	$-60 \le k \le 61$
	$-21 \le l \le 21$	$-27 \le l \le 20$	$-76 \le l \le 73$
θ_{max} [°]	36.455	80.949	81.008
Reflections collected	144720	139588	146520
Independent reflections	26619	11292	9180
R_{int}	0.0421	0.0764	0.0654
Refined parameters	1039	928	573
R_1 [$I > 2\sigma(I)$]	0.0639	0.0417	0.0770
wR_2 [all data]	0.1681	0.1170	0.2211
x(Flack)	0.33(2)	–	–
GooF	1.099	1.042	1.064
$\Delta\rho_{final}$ (max/min) [e·Å^{-3}]	5.049/-1.355	2.308/-1.889	0.484/-0.524

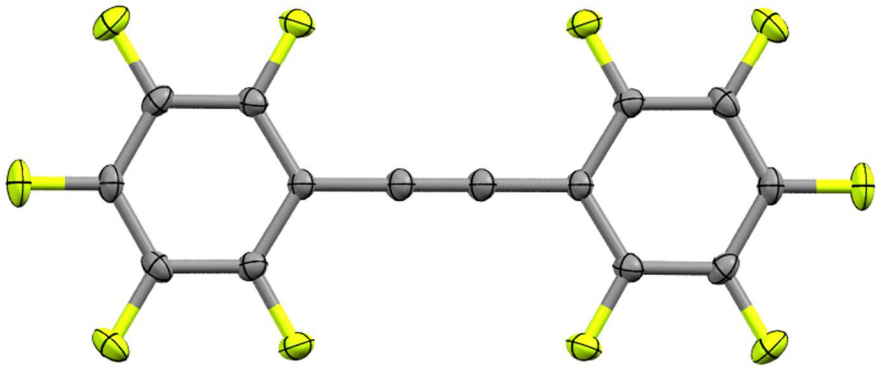

Figure S37. Molecular structure of bis(pentafluorophenyl)ethyne **B** in the solid state, crystallized from benzene. Ellipsoids are drawn at a probability level of 50%. CCDC-2246859

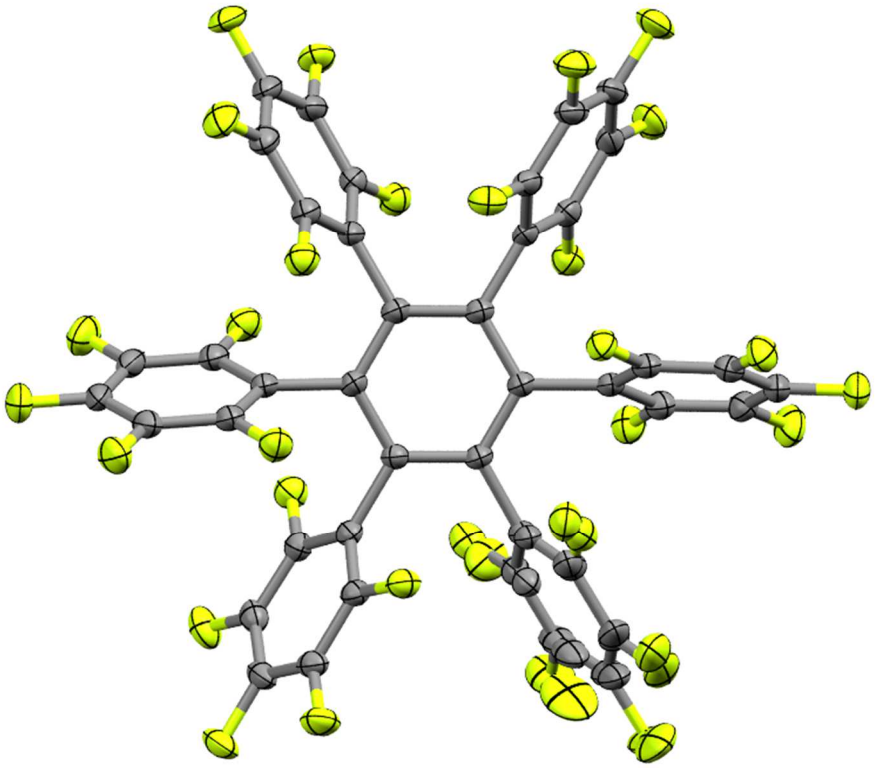

Figure S38. Molecular structure of hexakis(pentafluorophenyl)benzene in the solid state. Ellipsoids are drawn at a probability level of 50%. Hexakis(pentafluorophenyl)benzene was obtained as a by-product in the synthesis of **C** and crystallized from toluene/DCM. CCDC-2246860

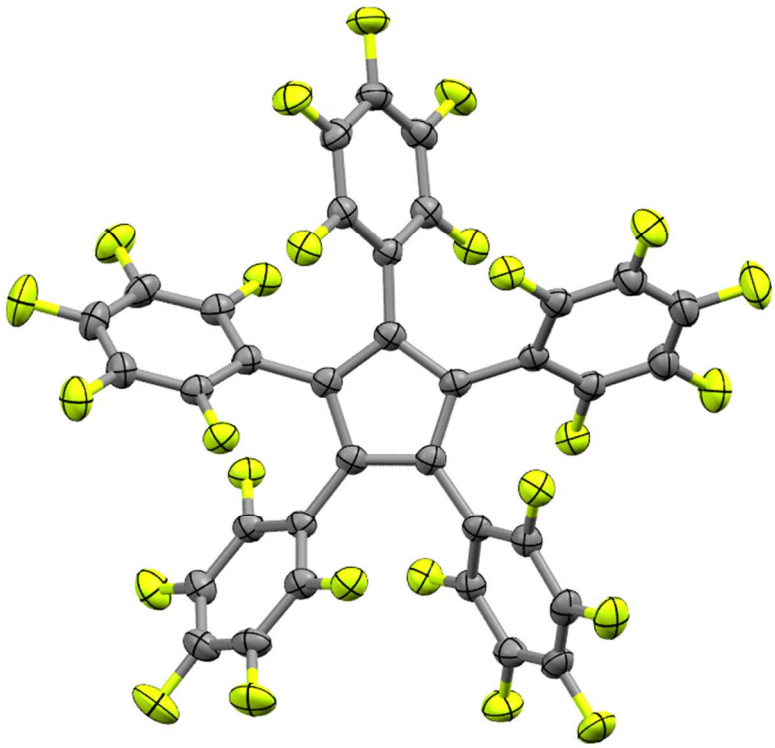

Figure S39. Molecular structure of pentakis(pentafluorophenyl)cyclopentadienyl radical **2a** in the solid state, crystallized from benzene. Ellipsoids are drawn at a probability level of 50%. CCDC-2246850

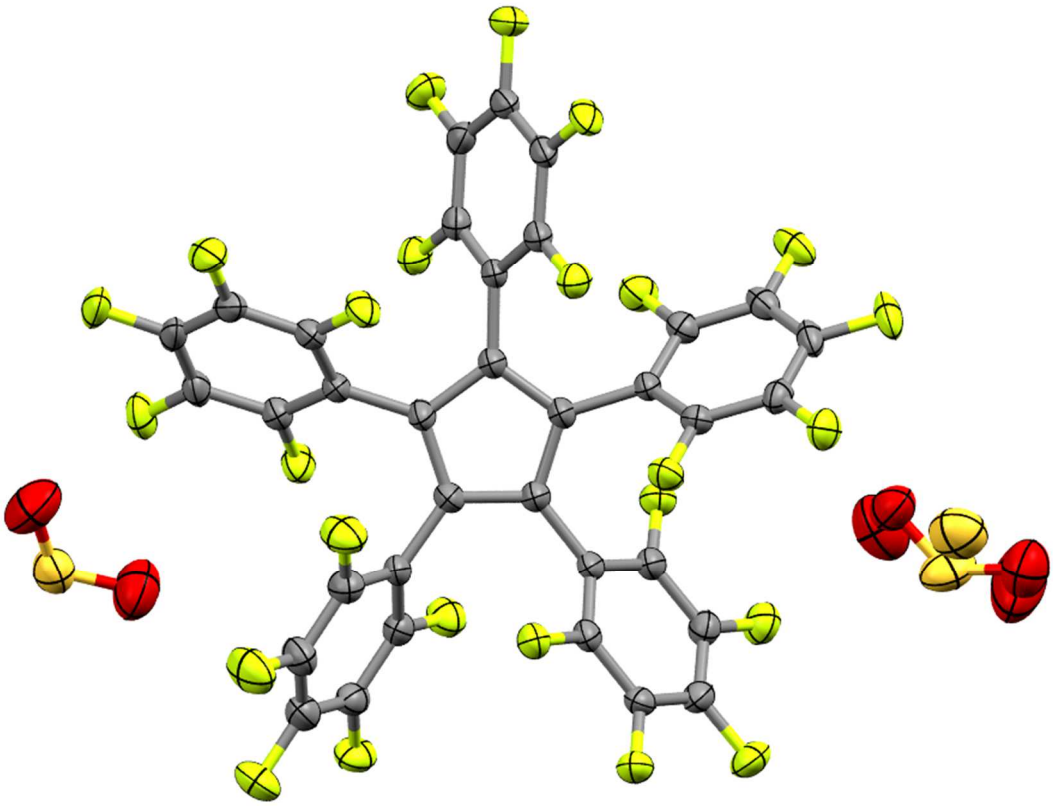

Figure S40. Molecular structure of pentakis(pentafluorophenyl)cyclopentadienyl radical **2b** in the solid state, crystallized from SO_2. Ellipsoids are drawn at a probability level of 50%. CCDC-2246851

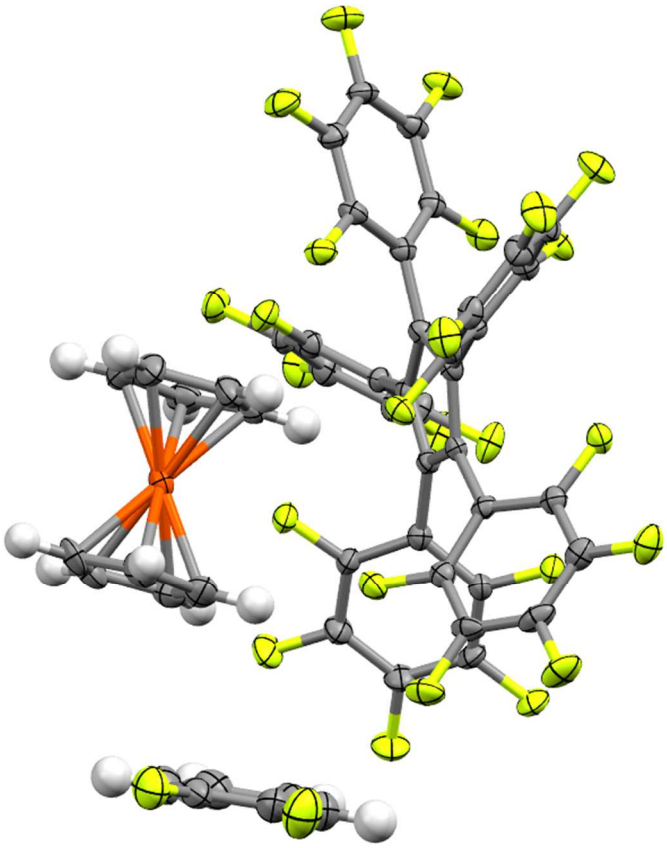

Figure S41. Molecular structure of ferrocenium pentakis(pentafluorophenyl)cyclopentadienide **3a** in the solid state, crystallized from 1,2-difluorobenzene/hexane. Ellipsoids are drawn at a probability level of 50%. CCDC-2246852

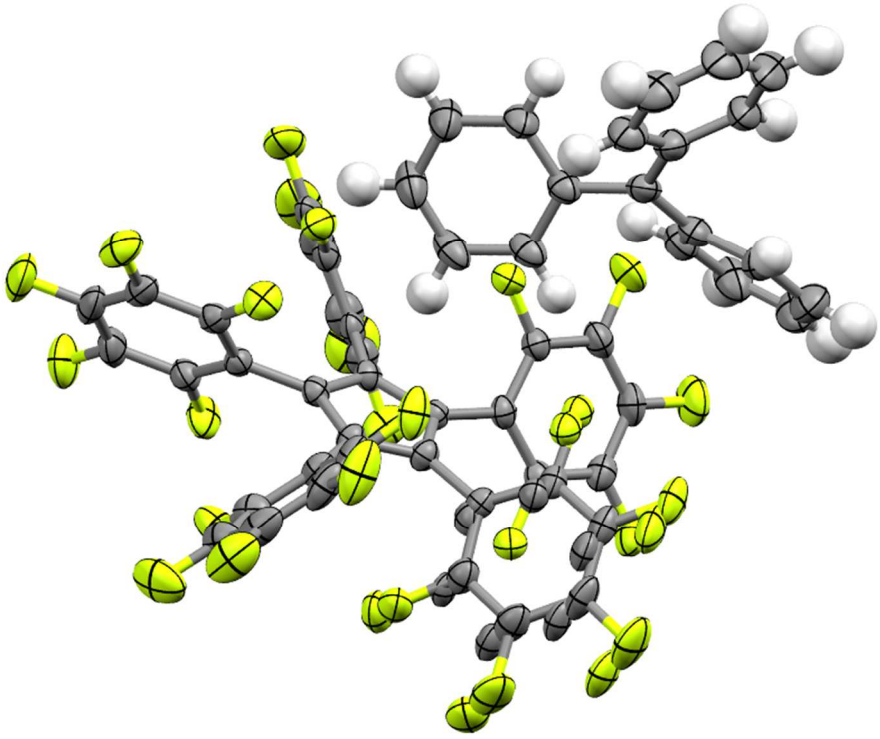

Figure S42. Molecular structure of tritylium pentakis(pentafluorophenyl)cyclopentadienide **3b** in the solid state, crystallized from toluene. Ellipsoids are drawn at a probability level of 50%. CCDC-2246853

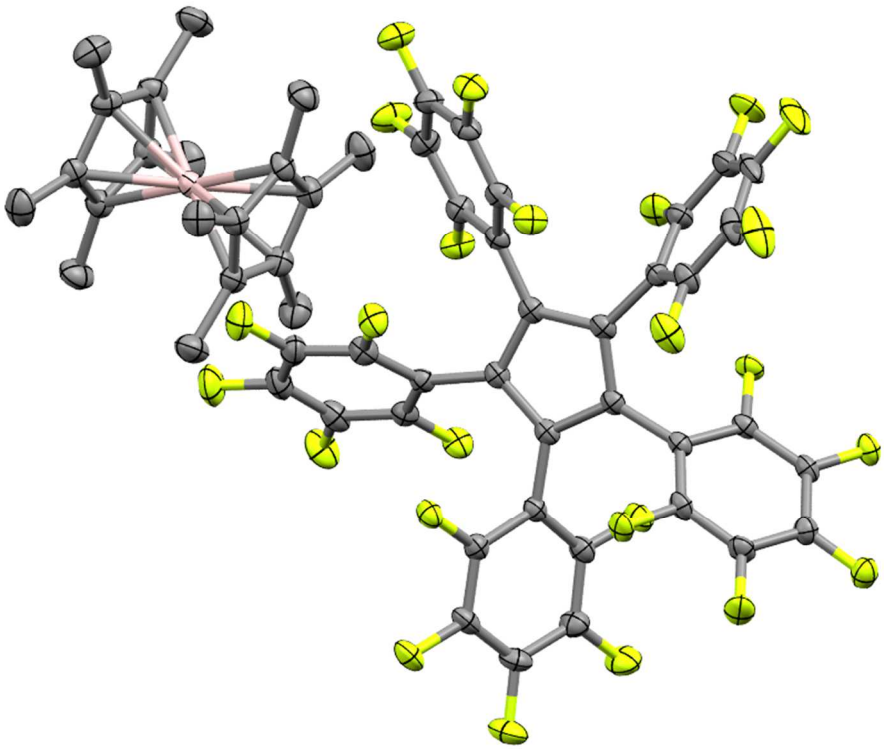

Figure S43. Molecular structure of decamethylaluminocenium pentakis(pentafluorophenyl)cyclopenta-dienide **3c** in the solid state, crystallized from benzene. Ellipsoids are drawn at a probability level of 50%. Hydrogen atoms are omitted for clarity. CCDC-2246854

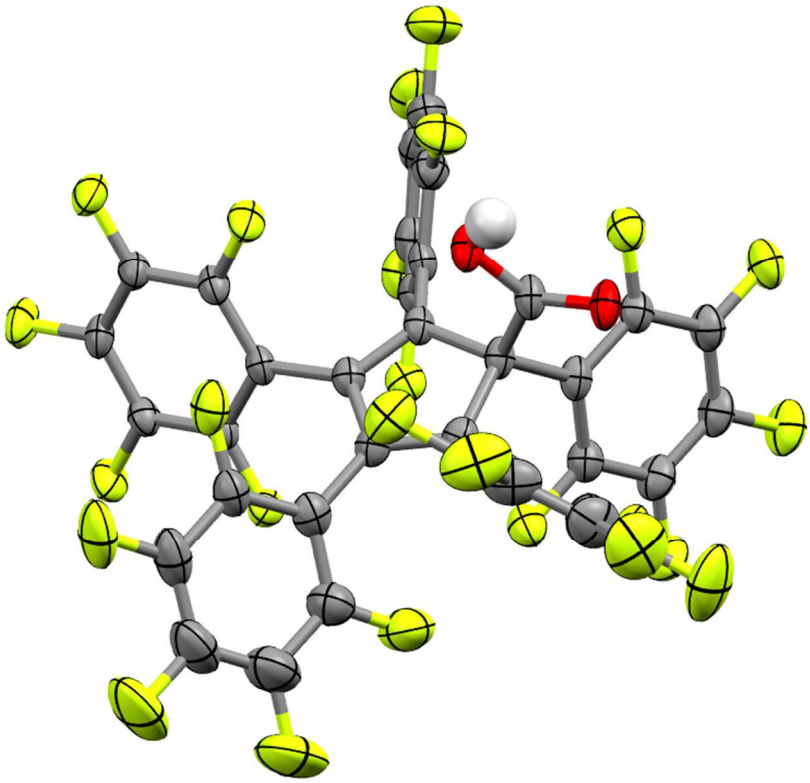

Figure S44. Molecular structure of pentakis(pentafluorophenyl)cyclopentadienylcarboxylic acid **5** in the solid state, crystallized from hexafluorobenzene/hexane. Ellipsoids are drawn at a probability level of 50%. CCDC-2246857

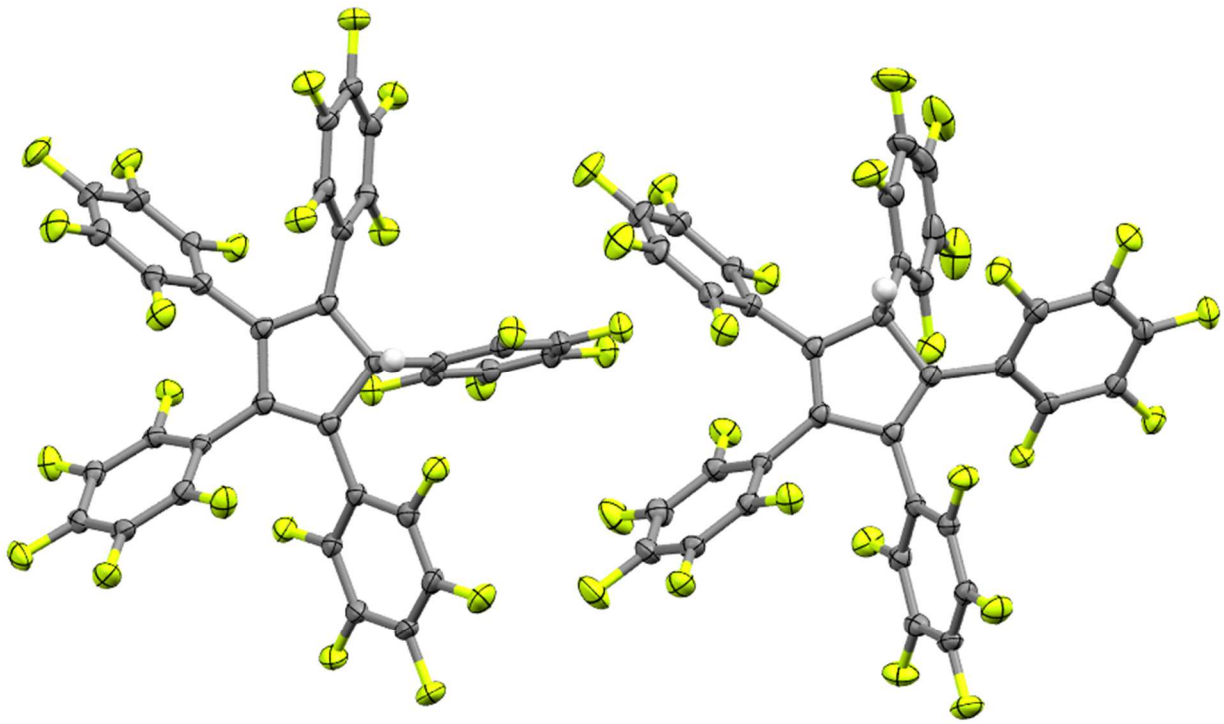

Figure S45. Asymmetric unit of pentakis(pentafluorophenyl)cyclopentadiene **6** in the solid state, featuring two independent molecules, crystallized from acetonitrile/hexane. Ellipsoids are drawn at a probability level of 50%. CCDC-2246858

Table S2. Bond lengths in the Cp ring and shortest distance of the Cp centroid to an adjacent hydrogen atom for **3a-c**.

	3a	**3b**	**3c**
bond length (Å) of C1-C2	1.405(5)	1.406(3)	1.409(3)
bond length (Å) of C2-C3	1.408(5)	1.409(3)	1.420(3)
bond length (Å) of C3-C4	1.415(6)	1.412(3)	1.401(3)
bond length (Å) of C4-C5	1.411(5)	1.409(3)	1.414(3)
bond length (Å) of C5-C1	1.405(5)	1.411(3)	1.411(3)
distance (Å) between centroid(Cp)-H	2.546	2.683	3.131

Section 2B

Supplied cif-files

CCDC-2246848 (**1a**+), CCDC-2246849 (**1b**+), CCDC-2246850 (**2a**), CCDC-2246851 (**2b**), CCDC-2246852 (**3a**), CCDC-2246853 (**3b**), CCDC-2246854 (**3c**), CCDC-2246857 (**5**), CCDC-2246858 (**6**), CCDC-2246859 (**B**), and CCDC-2246860 (**$C_6(C_6F_5)_6$**).

Checkcif Validation and Replies

_vrf_CRYSS02_**1b**+

PROBLEM: The value of _exptl_crystal_size_max is > 1.0

RESPONSE: The only available speciemen was too large for the X-ray beam and we did not want to risk losing it by trying to cut it. Any attempts to obtain a more suitable one yielded the other polymorph.

_vrf_PLAT971_**1b**+

PROBLEM: Check Calcd Resid. Dens.

RESPONSE: The uneven irrdiation of the crystal due to its large size led to distortions of the reflection intensities and consequently to problems with the absorption correction. Several methods and setting were tried but the residual electron density could not be reduced any further. Quantitative results should be carefully assessed and may be unreliable.

_vrf_PLAT934_**3b**

PROBLEM: Number of (Iobs-Icalc)/Sigma(W) > 10 Outliers .. 2 Check

RESPONSE: Iobs is larger than Icalc likely caused by background scattering of ice crystals that formed during the measurement. This also matches the theta range of the reflections.

IV. Computational Details

General. All calculations were performed by using the program packages Gaussian 16[11] and Amsterdam Density Functional (ADF)[12-13] and Orca 5.0.0[14]. DFT geometry optimizations were carried out using B3LYP[15-17] and CAM-B3LYP[18] for closed-shell species and the corresponding unrestricted versions UB3LYP and UCAM-B3LYP for open-shell species. To consider the dispersion interaction in an appropriate way, the additional dispersion correction with Becke-Johnson damping (D3BJ)[19] was employed. As basis sets 6-31G(d), 6-311++G(d,p) and TZP were applied. Furthermore, the open-shell singlet states were calculated using UB3LYP-D3BJ/6-31G(d), UCAM-B3LYP-D3BJ/6-31G(d) and UB3LYP-D3BJ/6-311++G(d,p) and the "guess = mix" keyword. In all cases, the restricted open-shell calculations gave the same energy values as the calculations of the corresponding closed-shell states. To treat relativistic effects the zeroth order regular approximation (ZORA)[20] to the Dirac equation was used for the B3LYP-D3BJ/TZP calculations. Frequency calculations were carried out at each of the structures to verify the nature of the stationary point. It turned out that all stationary states except of radical **2** have none imaginary frequency. However, the negative frequency in **2** has a mode of only 6 cm^{-1}.The UV spectra were simulated with time-dependent density functional theory (TD-DFT)[21], using the potential PBE0[22] and the basis set def2-TZVP. The energy, oscillator strength, and rotatory strength were calculated for each of the 20 lowest excitations. To take solvent effects into account, the solvent model SMD[23] (perfluorobenzene as solvent) was used for the calculations of the UV spectra.

A NICS-based scan was used as a magnetic criterion of aromaticity. Therefore, the NICS values were calculated using CAM-B3LYP/def2-TZVP//CAM-B3LYP-D3BJ/6-311++G(d,p) along a line perpendicular from the center of the ring plane to 5 Å, with a step size of 0.1 Å (Figure S43). Magnetic shieldings were calculated by employing the GIAO method[24].

The degree of (anti)aromaticity was further evaluated by using the harmonic oscillator model of aromaticity (HOMA)[25-26] index:

$$HOMA = 1 - \frac{\alpha}{n}\sum_{i}^{n}\left(R_{opt} - R_i\right)^2$$

In this equation, R_{opt} corresponds to the optimal bond length taken as 1.388 Å for a CC bond. R_i represents an individual bond length; n is the number of bonds taken up in the summation and α is an empirical constant (257.7 $Å^{-2}$).[26]

Single-point calculations were performed using the double hybrid method B2PLYP-D3BJ[27] and the TZ2P[28] basis set. Furthermore, the zeroth order regular approximation (ZORA)[20] to the Dirac equation was employed.

Furthermore, single-point calculations were conducted at the DLPNO-CCSD(T)[29] level of theory. As basis sets def2-SVP[30], cc-pVDZ[31], def2-TZVPP[30], cc-pVTZ[31] and def2-QZVPP[30] were applied. As auxiliary basis sets the /C[32] auxiliary basis sets were taken. To speed up the calculation the RIJCOSX[33] approximation was used, whereby def2/J[34] as auxiliary basis set was employed.

Conductor-like polarizable continuum model (CPCM)[35] was applied to determine the energy of the isodesmic reaction. The solvent SO_2 was defined by the dielectric constant (17.43) and the refractive index (1.3653).

The geometrical data for these single point calculations stem from the B3LYP-D3BJ/TZP calculations as well as from the X-ray structure analyses.

Table S3. Energy (ΔE) and Gibbs energy (ΔG) of the triplet state of $\mathbf{1}^+$ and $\mathbf{1}^+[\mathbf{SbF_6}]^-$ relative to the singlet state. The values are given in kcal/mol.

method	molecule	ΔE	ΔG
cam-B3LYP-D3BJ/6-31G(d)	$\mathbf{1}^+$	-6.20	-5.43
cam-B3LYP-D3BJ/6-311++G(d,p)	$\mathbf{1}^+$	-5.55	-4.58
B3LYP-D3BJ/6-31G*	$\mathbf{1}^+$	-5.62	-5.39
B3LYP-D3BJ/TZP[a]	$\mathbf{1}^+$	-4.96	-5.45
B3LYP-D3BJ/TZP[a]	$\mathbf{1}^+[\mathbf{SbF_6}]^-$	-3.65	-2.54
B2PLYP-D3BJ/TZ2P//B3LYP-D3BJ/TZP[a]	$\mathbf{1}^+$	-2.27	-2.77
B2PLYP-D3BJ/TZ2P//B3LYP-D3BJ/TZP[a]	$\mathbf{1}^+[\mathbf{SbF_6}]^-$	-0.75	+0.36

[a] The zeroth order regular approximation (ZORA) to the Dirac equation was used.

Table S4. Energy (ΔE) of the triplet state of $\mathbf{1}^+$ relative to the singlet state. The geometrical data for these single point calculations stem from the B3LYP-D3BJ/TZP calculations. The values are given in kcal/mol.

method	ΔE
DLPNO-CCSD(T)/def2-SVP	-5.8
DLPNO-CCSD(T)/cc-pVDZ	-5.9
DLPNO-CCSD(T)/def2-TZVPP	-6.4
DLPNO-CCSD(T)/cc-pVTZ	-5.8
DLPNO-CCSD(T)/def2-QZVPP	-5.6

Table S5. Energy (ΔE) of the triplet state relative to the singlet state. The geometrical data for these single point calculations stem from the X-ray structure analyses. The values are given in kcal/mol.

method	molecule	ΔE
B3LYP-D3BJ/TZP	**1a**$^{+}$•**[Sb$_3$F$_{16}$]**$^{-}$	+0.6
	1b^{+}•**[Sb$_3$F$_{16}$]**$^{-}$	+5.0
B2PLYP-D3BJ/TZ2P	**1a**$^{+}$•**[Sb$_3$F$_{16}$]**$^{-}$	+4.2
	1b^{+}•**[Sb$_3$F$_{16}$]**$^{-}$	+8.1
DLPNO-CCSD(T)/def2-SVP	**1a**$^{+}$•**[Sb$_3$F$_{16}$]**$^{-}$	+3.0
	1b^{+}•**[Sb$_3$F$_{16}$]**$^{-}$	+6.7
DLPNO-CCSD(T)/def2-TZVPP	**1a**$^{+}$•**[Sb$_3$F$_{16}$]**$^{-}$	+2.4
	1b^{+}•**[Sb$_3$F$_{16}$]**$^{-}$	+6.5

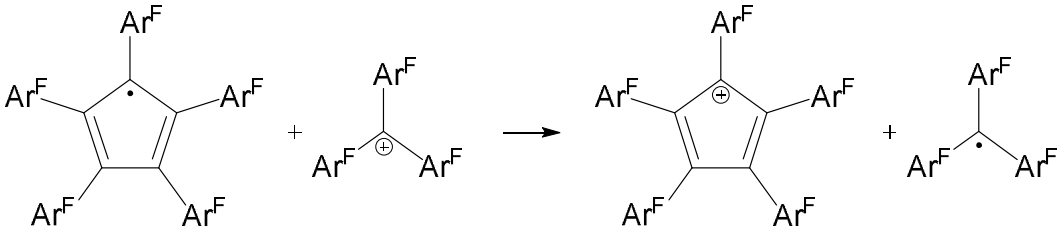

Table S6. Energy (ΔE) of the above shown isodemic reaction. The geometrical data for these single point calculations stem from the B3LYP-D3BJ/TZP calculations. The values are given in kcal/mol.

method	ΔE
B3LYP-D3BJ/TZP	+14.3
B2PLYP-D3BJ/TZ2P	+16.6
DLPNO-CCSD(T)/def2-SVP(CPCM,SO_2)	+21.6
DLPNO-CCSD(T)/def2-TZVPP(CPCM,SO_2)	+21.7
DLPNO-CCSD(T)/cc-pVTZ(CPCM,SO_2)	+21.7

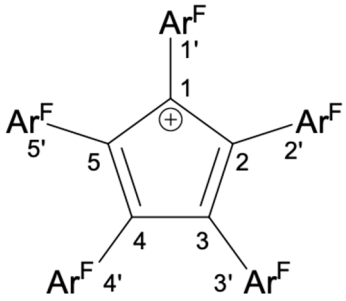

1

Figure S46. Assignment of atom labels.

Table S7. Bond distances [Å] in the singlet und triplet state of $\mathbf{1}^+$ and $\mathbf{1}^+[\mathbf{SbF_6}]^-$ calculated by means of B3LYP-D3BJ/TZP(ZORA).

bond	**1**		**1 SbF_6**	
	singlet	triplet	singlet	triplet
C1-C2	1.458	1.431	1.460	1.431
C2-C3	1.366	1.431	1.365	1.429
C3-C4	1.539	1.434	1.532	1.430
C4-C5	1.371	1.434	1.354	1.432
C5-C1	1.453	1.433	1.474	1.432
C1-C1’	1.434	1.455	1.426	1.454
C2-C2’	1.471	1.455	1.474	1.456
C3-C3’	1.449	1.455	1.451	1.457
C4-C4’	1.446	1.454	1.456	1.455
C5-C5’	1.471	1.454	1.468	1.454

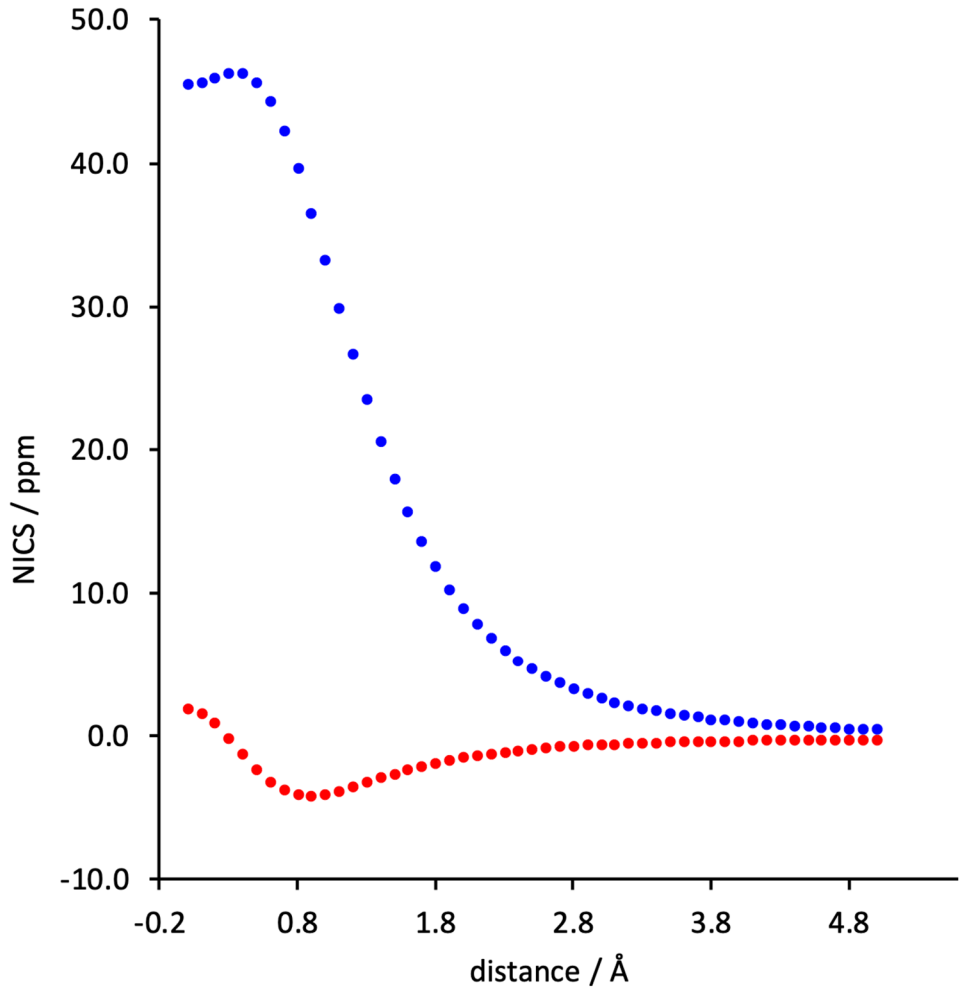

Figure S47. NICS scans of $\mathbf{1}^{+}$ calculated using CAM-B3LYP/def2-TZVP//CAM-B3LYP-D3BJ/6-311++G(d,p). Blue-colored curve refers to singlet state and red-colored curve refers to triplet state.

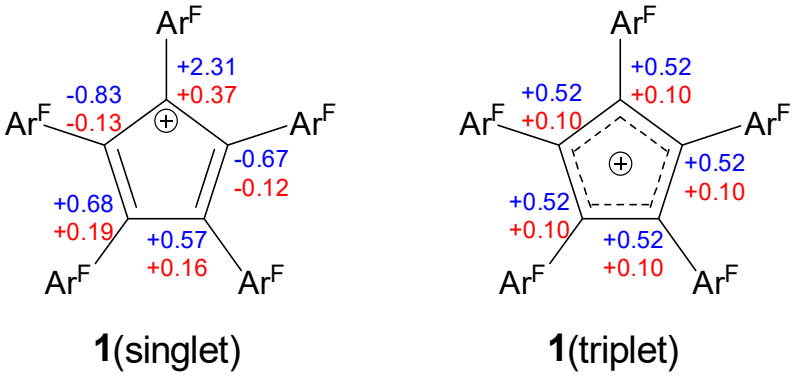

Figure S48. APT (atomic polar tensor) charges (blue; CAM-B3LYP-D3BJ/6-311++G(d,p)) and NBO (natural bond orbitals) charges (red; CAM-B3LYP/def2-TZVP//CAM-B3LYP-D3BJ/6-311++G(d,p)) of $\mathbf{1}^{+}$ in the singlet (left) und triplet (right).

Calculated HIA and FIA of 1

Gas phase:

The structures of Me_3SiH, Me_3SiF, Me_3Si^+, $[Cp(C_6F_5)_5]^+$ (singlet), Cp $(C_6F_5)_5H$ and $Cp(C_6F_5)_5F$ were optimized using B3LYP-D3(BJ)/def2-TZVPP. To determine the hydride ion affinity (HIA) / fluoride ion affinity (FIA), differences between the „sum of electronic and zero-point energies" were calculated for the reactions:

$[Cp(C_6F_5)_5]^+$ (Singlet) + Me_3SiF → $Cp(C_6F_5)_5F$ + Me_3Si^+

-3830.678637 + (-509.220634) → -3930.857051 + (-408.973937) Hartree

- 4339.899271 → - 4339.830988 Hartree (1 Hartree = 2625 kJ/mol)

The reaction is 179 kJ/mol endothermic. The fluoride affinity of $Cp(C_6F_5)_5^+$ (singlet) is 179 kJ/mol lower than of Me_3Si^+.

$[Cp(C_6F_5)_5]^+$ (Singlet) + Me_3SiH → $Cp(C_6F_5)_5H$ + Me_3Si^+

-3830.678637 + (-409.850856) → -3831.589902 + (-408.973937) Hartree

-4240.529493 → 4240.563839 Hartree (1 Hartree = 2625 kJ/mol)

The reaction is 90 kJ/mol exothermic. The hydride affinity of $Cp(C_6F_5)_5^+$ (singlet) is 90 kJ/mol higher than of Me_3Si^+.

The Me_3SiX (X = H, F)/Me_3Si^+ pair has been established in the literature as a reliable anchorpoint to calculate hydride and fluoride ion affinities of other Lewis acids. The fluoride affinity of the Me_3Si^+ cation has been calculated to be 952.5 kJ/mol (CCSD(T)/CBS) [36] The hydride affinity of Me_3Si^+ calculated with the same method is 924 kJ/mol.[37]

Since the hydride abstraction from Me_3SiH is exothermic by 90 kJ/mol, the hydride ion affinity of $Cp(C_6F_5)_5^+$ (singlet) is 1014 kJ/mol. Since the fluoride abstraction from Me_3SiF is endothermic by 179 kJ/mol, the fluoride ion affinity of $Cp(C_6F_5)_5^+$ (singlet) is 774 kJ/mol .

To estimate the influence of the solvent on the FIAs and HIAs, structures were optimized with B3LYP-D3(BJ)/def2-TZVPP, using the PCM solvent model and dielectric constants of ε=9 for CH_2Cl_2 and ε=13 for SO_2. The FIA and HIA values effected by solvation were calculated using the procedure described in the literature.[38]

$FIA_{solv} = FIA(gas\ phase) - \Delta E_{solv}(LA\text{-}F^-) + \Delta E_{solv}(LA) + \Delta E_{solv}(F^-)$

$FIA_{solv} = FIA(Cp^+\ gas\ phase) - \Delta E_{solv}(Cp\text{-}F) + \Delta E_{solv}(Cp^+) + \Delta E_{solv}(F^-)$

FIA_{DCM}= 774 – (–32) +(–165) +(– 331) kJ/mol= **310 kJ/mol**

FIA_{SO2}= FIA 774 – (–34) + (– 173) + (– 344) = **291 kJ/mol**

$HIA_{solv} = HIA(gas\ phase) - \Delta E_{solv}(LA\text{-}H^-) + \Delta E_{solv}(LA) + \Delta E_{solv}(H^-)$

$HIA_{solv} = HIA - \Delta E_{solv}(Cp\text{-}H) + \Delta E_{solv}(Cp^+) + \Delta E_{solv}(H^-)$

HIA_{DCM}: 1014 – (–32) +(– 165) +(– 339) kJ = **542 kJ/mol**

HIA_{SO2}: 1014 – (–34) + (– 173) +(– 352) kJ = **523 kJ/mol**

For comparison:

FIA of SbF_5 in the gas phase using B3LYP-D3(BJ)/def2-TZVPP.:

$SbF_5 + Me_3SiF \rightarrow SbF_6^- + Me_3Si^+$

-739.851430 + (-509.220634) → -839.926356 + (-408.973937) Hartree

-1249.072064 Hartree → -1248.900293 Hartree (1 Hartree = 2625 kJ/mol)

The reaction is 451 kJ/mol endothermic. The fluoride affinity of SbF_5 is 451 kJ/mol lower than of Me_3Si^+. Since the FIA of Me_3Si^+ is 952.5 kJ/mol the FIA of SbF_5 in the gas phase is 502 kJ/mol.

FIA of SbF_5 in solution:

$FIA_{solv} = FIA(\text{gas phase}) - \Delta E_{solv}(LA\text{-}F^-) + \Delta E_{solv}(LA) + \Delta E_{solv}(F^-)$

$FIA_{solv} = FIA(SbF_5) - \Delta E_{solv}(SbF_6^-) + \Delta E_{solv}(SbF_5) + \Delta E_{solv}(F^-)$

FIA_{DCM}= 502 – (–188) +(–16) +(– 331) kJ/mol= **343 kJ/mol**

FIA_{SO2}= 502 – (–196) + (– 17) + (– 344) kJ/mol = **337 kJ/mol**

The FIA of SbF_5 in the gas phase (502 kJ/mol) decreases to 343 kJ/mol in CH_2Cl_2 and 337 kJ/mol in SO_2.

Literature values for comparison: The FIA of SbF_5 in the gas phase (496 kJ/mol) decreases to 362 kJ/mol in CH_2Cl_2.[38]

V. Side Reactions

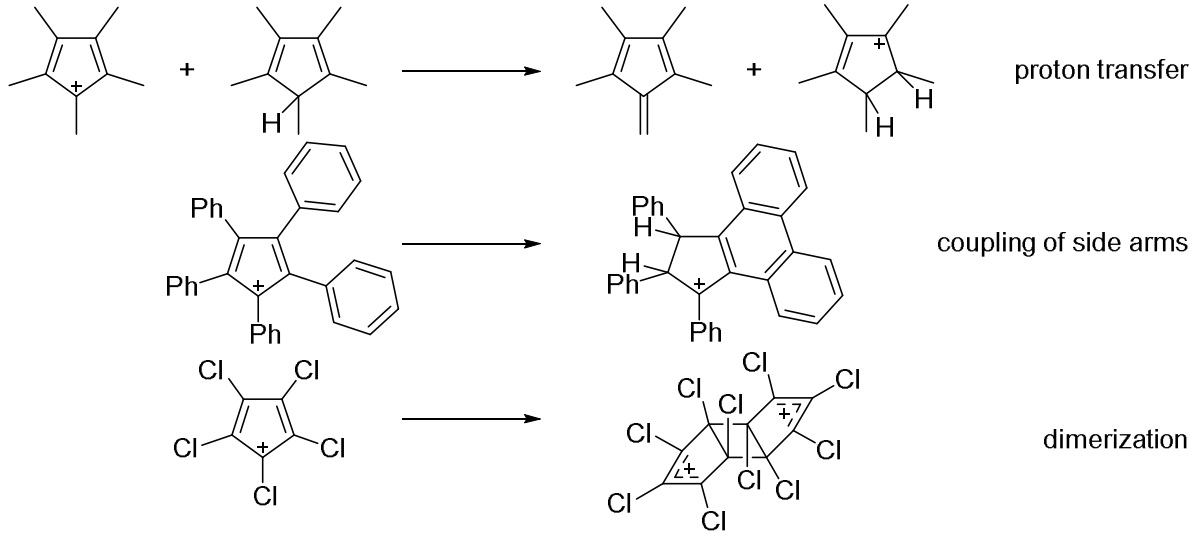

Scheme S49: Examples of side reactions that hindered the isolation of Cp cations.[39-45]

VI. References

1. Willstätter, R. & Waser, E. Über Cyclooctatetraen. *Ber. Dtsch. Chem. Ges.* **44**, 3423–3445; 10.1002/cber.191104403216 (1911).

2. Webb, A. F. & Gilman, H. Reactions of some perhaloarenes with metals and metal halides. *J. Organomet. Chem.* **20**, 281–283; 10.1016/S0022-328X(00)80121-7 (1969).

3. Birchall, J. M., Bowden, F. L., Haszeldine, R. N. & Lever, A. B. P. Polyfluoroarenes. Part IX. Decafluorotolan: synthesis, properties, and use as an organometallic ligand. *J. Chem. Soc., A,* 747; 10.1039/j19670000747 (1967).

4. Inés, B., Holle, S., Bock, D. & Alcarazo, M. Polyfluorinated Cyclopentadienones as Lewis Acids. *Synlett* **25**, 1539–1541 (2014).

5. Burns, C. T., Shapiro, P. J., Budzelaar, P. H. M., Willett, R. & Vij, A. Bis(permethylcyclopentadienyl)aluminum Compounds: Precursors to $[Cp^*_2Al]^+$ but Not to Cp^*_3Al. *Organometallics* **19**, 3361–3367; 10.1021/om000173x (2000).

6. Boeré, R. T. *et al.* Oxidation of closo-$B_{12}Cl_{12}$- to the radical anion $B_{12}Cl_{12}$*- and to neutral $B_{12}Cl_{12}$. *Angew. Chem. Int. Ed. Engl.* **50**, 549–552 (2011).

7. Sheldrick, G. M. Phase annealing in SHELX-90: direct methods for larger structures. *Acta Cryst.* **46**, 467–473 (1990).

8. Sheldrick, G. M. SHELXL-2017, Program for the Refinement of Crystal Structures University of Göttingen, Göttingen (Germany) (2017). See also: Sheldrick, G. M. Crystal structure refinement with SHELXL, *Acta Cryst.,* **C71**, 3-8 (2015).

9. Hübschle, C. B., Sheldrick, G. M. & Dittrich, B. ShelXle: a Qt graphical user interface for SHELXL. *J. Appl. Cryst.* **44**, 1281–1284 (2011).

10. van der Sluis, P. & Spek, A. L. BYPASS: an effective method for the refinement of crystal structures containing disordered solvent regions. *Acta Crystallogr A Found Crystallogr* **46,** 194–201; 10.1107/S0108767389011189 (1990).

11. Frisch, M. J. *et al.* Gaussian 16, Revision A.03, Wallingford CT, (2016).

12. te Velde, G. *et al.* Chemistry with ADF. *J. Comput. Chem.* **22**, 931–967 (2001).

13. Baerends, E. J. *et al.* ADF 2020.1, SCM, Theoretical Chemistry, Vrije Universiteit, Amsterdam, The Netherlands, http://www.scm.com, **2020**.

14. Neese, F. Software Update: The ORCA Program System—Version 5.0. *WIREs Comput. Mol. Sci.* **12**, e1606 (2022).

15. Becke, A. D. Density-functional exchange-energy approximation with correct asymptotic behavior. *Phys. Rev. A* **38**, 3098–3100 (1988).

16. Lee, C., Yang, W. & Parr, R. G. Development of the Colle-Salvetti correlation-energy formula into a functional of the electron density. *Phys. Rev. B* **37,** 785–789 (1988).

17. Miehlich, B., Savin, A., Stoll, H. & Preuss, H. Results obtained with the correlation energy density functionals of becke and Lee, Yang and Parr. *Chem. Phys. Lett.* **157**, 200–206 (1989).

18. Yanai, T., Tew, D. P. & Handy, N. C. A new hybrid exchange–correlation functional using the Coulomb-attenuating method (CAM-B3LYP). *Chem. Phys. Lett.* **393**, 51–57 (2004).

19. Grimme, S., Ehrlich, S. & Goerigk, L. Effect of the damping function in dispersion corrected density functional theory. *J. Comp. Chem.* **32**, 1456–1465 (2011).

20. van Lenthe, E., Ehlers, A. & Baerends, E.-J. Geometry optimizations in the zero order regular approximation for relativistic effects. *J. Chem. Phys.* **110**, 8943–8953 (1999).

21. Furche, F. & Ahlrichs, R. Adiabatic time-dependent density functional methods for excited state properties. *J. Chem. Phys.* **117**, 7433-7447 (2002).

22. Adamo, C. & Barone, V. Toward reliable density functional methods without adjustable parameters: The PBE0 model. *J. Chem. Phys.* **110**, 6158-6170 (1999).

23. Marenich, A. V., Cramer, C. J. & Truhlar, D. G. Universal Solvation Model Based on Solute Electron Density and on a Continuum Model of the Solvent Defined by the Bulk Dielectric Constant and Atomic Surface Tensions. *J. Phys. Chem. B* **113**, 6378-6396 (2009).

24. Wolinski, K., Hinton, J. F. & Pulay, P. Efficient implementation of the gauge-independent atomic orbital method for NMR chemical shift calculations. *J. Am. Chem. Soc.* **112**, 8251–8260 (1990).

25. Julg, A. & Franois, P. Recherches sur la géométrie de quelques hydrocarbures non-alternants: son influence sur les énergies de transition, une nouvelle définition de l'aromaticité. *Theoret. Chim. Acta* **8**, 249–259 (1967).

26. Krygowski, T. M. & Cyrański, M. Separation of the energetic and geometric contributions to the aromaticity of π-electron carbocyclics. *Tetrahedron* **52**, 1713–1722 (1996).

27. Grimme, S. Semiempirical hybrid density functional with perturbative second-order correlation. *J. Chem. Phys.* **124**, 34108 (2006).

28. van Lenthe, E. & Baerends, E. J. Optimized Slater-type basis sets for the elements 1-118. *J. Comput. Chem.* **24**, 1142–1156 (2003).

29. Riplinger, C., Sandhoefer, B., Hansen, A. & Neese, F. Natural Triple Excitations in Local Coupled Cluster Calculations with Pair Natural Orbitals. *J. Chem. Phys.* **139**, 134101 (2013).

30. Weigend, F. & Ahlrichs, R. Balanced Basis Sets of Split Valence, Triple Zeta Valence and Quadruple Zeta Valence Quality for H to Rn: Design and Assessment of Accuracy. *Phys. Chem. Chem. Phys.* **7**, 3297-3305 (2005).

31. Dunning Jr., T. H. Gaussian basis sets for use in correlated molecular calculations. I. The atoms boron through neon and hydrogen. *J. Chem. Phys.* **90**, 1007-1023 (1989).

32. Hellweg, A., Hättig, C., Höfener, S. & Klopper, W. Optimized Accurate Auxiliary Basis Sets for RI-MP2 and RI-CC2 Calculations for the Atoms Rb to Rn. *Theor. Chem. Acc.* **117**, 587-597 (2007).

33. Neese, F., Wennmohs, F., Hansen, A. & Becker, U. Efficient, Approximate and Parallel Hartree–Fock and Hybrid DFT Calculations. A 'Chain-of-Spheres' Algorithm for the Hartree–Fock Exchange. *Chem. Phys.* **356**, 98-109 (2009).

34. Weigend, F. Accurate Coulomb-Fitting Basis Sets for H to Rn. *Phys. Chem. Chem. Phys.* **8**, 1057-1065 (2006).

35. Barone, V. & Cossi, M. Quantum Calculation of Molecular Energies and Energy Gradients in Solution by a Conductor Solvent Model. *J. Phys. Chem. A* **102**, 1995-2001 (1998).

36. Erdmann, P., Leitner, Schwarz, J. & Greb, L. An Extensive Set of Accurate Fluoride Ion Affinities for *p*-Block Element Lewis Acids and Basic Design Principles for Strong Fluoride Ion Acceptors. *ChemPhysChem* **21**, 987-994 (2020).

37. Erdmann, P., Greb, L. Multidimensional Lewis Acidity: A Consistent Data Set of Chloride, Hydride, Methide, Water and Ammonia Affinities for 183 p-Block Element Lewis Acids. *ChemPhysChem* **22**, 935-943 (2021).

38. Erdmann, P., Leitner, Schwarz, J. & Greb, L. An Extensive Set of Accurate Fluoride Ion Affinities for *p*-Block Element Lewis Acids and Basic Design Principles for Strong Fluoride Ion Acceptors. *ChemPhysChem* **21**, 987-994 (2020).

39. Otto, M. *et al.* The Stable Pentamethylcyclopentadienyl Cation Remains Unknown. *Angew. Chem. Int. Ed. Engl.* **41**, 2275 (2002).

40. Lambert, J. B., Lin, L. & Rassolov, V. The Stable Pentamethylcyclopentadienyl Cation. *Angew. Chem. Int. Ed. Engl.* **41,** 1429–1431 (2002).

41. Breslow, R. & Chang, H. W. The Rearrangement of the Pentaphenylcyclopentadienyl Cation. *J. Am. Chem. Soc.* **83**, 3727-3728 (1961).

42. Rupf, S. M., Pröhm, P. & Malischewski, M. The 2+2 cycloaddition product of perhalogenated cyclopentadienyl cations: structural characterization of salts of the C10Cl102+ and C10Br102+ dications. *Chem. Commun.* **56**, 9834-9837 (2020).

43. Jones, J. N., Cowley, A. H. & Macdonald, C. L. B. The crystal structure of the 'pentamethylcyclopentadienyl cation' is that of the pentamethylcyclopentenyl cation. *Chem. Commun.,* 1520–1521 (2002).

44. Müller, T. Comment on the X-Ray Structure of Pentamethylcyclopentadienyl Cation. *Angew. Chem. Int. Ed. Engl.* **41**, 2276-2278 (2002).

45. Lambert, J. B. Statement. *Angew. Chem. Int. Ed. Engl.* **41**, 2278 (2002).